Ore Geology Reviews 87 (2017) 25–40

Contents lists available at ScienceDirect

Ore Geology Reviews

journal homepage: www.elsevier.com/locate/oregeorev

Formation of Fe-Mn crusts within a continental margin environment

Tracey Conrad [a,*], James R. Hein [b], Adina Paytan [a], David A. Clague [c]

[a] University California Santa Cruz, 1156 High Street, Santa Cruz, CA 95060, USA
[b] U.S. Geological Survey, PCMSC, 2885 Mission St., Santa Cruz, CA 95060, USA
[c] Monterey Bay Aquarium Research Institute, 7700 Sandholdt Rd., Moss Landing, CA 95039, USA

ARTICLE INFO

Article history:
Received 7 April 2016
Accepted 8 September 2016
Available online 9 September 2016

Keywords:
Ferromanganese crusts
Eastern Pacific
California margin
Strategic metals
Marine mineral resources

ABSTRACT

This study examines Fe-Mn crusts that form on seamounts along the California continental-margin (CCM), within the United States 200 nautical mile exclusive economic zone. The study area extends from approximately 30° to 38° North latitudes and from 117° to 126° West longitudes. The area of study is a tectonically active northeast Pacific plate boundary region and is also part of the North Pacific Subtropical Gyre with currents dominated by the California Current System. Upwelling of nutrient-rich water results in high primary productivity that produces a pronounced oxygen minimum zone. Hydrogenetic Fe-Mn crusts forming along the CCM show distinct chemical and mineral compositions compared to open-ocean crusts. On average, CCM crusts contain more Fe relative to Mn than open-ocean Pacific crusts. The continental shelf and slope release both Fe and Mn under low-oxygen conditions. Silica is also enriched relative to Al compared to open-ocean crusts. This is due to the North Pacific silica plume and enrichment of Si along the path of deep-water circulation, resulting in Si enrichment in bottom and intermediate waters of the eastern Pacific.

The CCM Fe-Mn crusts have a higher percentage of birnessite than open-ocean crusts, reflecting lower dissolved seawater oxygen that results from the intense coastal upwelling and proximity to zones of continental slope pore-water anoxia. Carbonate fluorapatite (CFA) is not present and CCM crusts do not show evidence of phosphatization, even in the older sections. The mineralogy indicates a suboxic environment under which birnessite forms, but in which pH is not high enough to facilitate CFA deposition. Growth rates of CCM crusts generally increase with increasing water depth, likely due to deep-water Fe sources mobilized from reduced shelf and slope sediments.

Many elements of economic interest including Mn, Co, Ni, Cu, W, and Te have slightly or significantly lower concentrations in CCM crusts relative to crusts from the Pacific Prime Crust Zone and other open-ocean basins. However, concentrations of total rare earth elements and yttrium average only slightly lower contents and in the future may be a strategic resource for the U.S.

1. Introduction

Hydrogenetic ferromanganese (Fe-Mn) crusts and nodules precipitate from seawater on elevated seafloor features devoid of sediment. Fe-Mn crusts have growth rates typically ranging from 1–5 mm/Myr (75% of analyzed open-ocean samples), with very high mean porosity of 60%, and extremely high mean specific surface area of 325 m^2/g (Hein et al., 2000). Fe-Mn crusts up to 26 cm thick that accumulated over 80 Ma have been found in the central Pacific Ocean (Hein et al., 2000; Hein and Koschinsky, 2014). The main manganese mineral in Fe-Mn crusts is vernadite (δ-MnO_2), which has a negative surface charge in seawater that can sorb positively charged ions from seawater (Koschinsky and Halbach, 1995; Koschinsky and Hein, 2003). The main iron mineral is Fe oxyhydroxide (FeO(OH)) that has a slight positive surface charge in seawater that is conducive to sorption of negatively charged ions and neutral complexes from seawater (Koschinsky and Hein, 2003). These properties of Fe-Mn crusts result in their enrichment in many elements relative to the Earth's crustal abundance (Hein et al., 2000, 2010a; Koschinsky and Hein, 2003). The most notable of these are Te, Co, Mo, Bi, Pt, Nb, W, Zr, and rare earth elements plus yttrium (REY) (Hein et al., 2000; Hein and Koschinsky, 2014).

Much of the research on Fe-Mn crusts has focused on open-ocean crusts from the equatorial Pacific (Hein et al., 2009). Fe-Mn crusts from the Pacific prime crust zone (PCZ) in the north-equatorial Pacific have the greatest economic potential and four exploration contracts

Abbreviations: Fe-Mn, ferromanganese; CCM, California continental margin; EEZ, exclusive economic zone; CCS, California Current System; NPIW, North Pacific Intermediate Water; CFA, carbonate fluorapatite; OMZ, oxygen minimum zone; PCZ, Pacific prime crust zone; CCZ, Clarion Clipperton Zone; PGE, platinum group elements; ppb, parts per billion; ppm, parts per million; REE, rare earth elements; REY, rare earth elements plus yttrium; HREY, heavy REY; CL, confidence level; ROV, remotely operated vehicle; PAAS, post-Archean Australian Shale.

* Corresponding author.
E-mail address: tconrad@ucsc.edu (T. Conrad).

http://dx.doi.org/10.1016/j.oregeorev.2016.09.010
0169-1368/

have been signed through the International Seabed Authority in that region (Hein et al., 2013, 2016). One exploration contract for Fe-Mn crusts from the Rio Grande Rise in the Atlantic Ocean has also been signed. There are fewer detailed studies of Fe-Mn crusts from the Atlantic and Indian Oceans with the exception of the northeast and northwest Atlantic Ocean (Koschinsky and Halbach, 1995; Muiños et al., 2013) and the Indian Ocean Afanasiy-Nikitin seamount complex (Banakar et al., 2007; Rajani et al., 2005) and Ninetyeast Ridge (Hein et al., 2016). Only a few studies have focused solely on continent-proximal Fe-Mn crusts from the east Pacific off southern California and within the Borderland (Hein et al., 2005, 2010a).

The California continental margin (CCM) is subject to relatively large terrestrial inputs, metal fluxes from continental shelf and slope hypoxic sediments, seasonal upwelling, high primary productivity, and a well-developed oxygen minimum zone (OMZ) (Hein et al., 2000). All of these CCM characteristics influence the formation of Fe-Mn crusts. This study looks at Fe-Mn crusts within the 200 nmi U.S. EEZ from central to southern California along the CCM (Fig. 1). Samples were collected on USGS cruises F6-87-NC, F7-87-SC, and MBARI cruises in 2000, 2003, 2004, and 2010 from the following edifices: Adam, Hoss, Ben, Little Joe, San Marcos, San Juan, Rodriguez, Davidson, Guide, Pioneer, Gumdrop, and Taney (A–D) seamounts and Northeast Bank, Patton Escarpment, and Santa Lucia Escarpment. USGS Open File Report 2010-1069 (Hein et al., 2010b), provides sample data from USGS cruise F7-87-SC for six of the fifteen seamounts and includes 64 of the samples encompassed in this study. Four of the five samples from the Santa Lucia Escarpment, USGS cruise F6-87-NC, are presented by Gibbs et al. (1993). Data from crusts collected on MBARI 2003 and 2004 cruises were included in the mean CA margin data presented in Hein et al. (2013) and Hein and Koschinsky (2014). Fe-Mn crust data from the Taney Seamounts, MBARI cruises 2000 and 2010, have not been previously published.

2. Setting

The CCM is a tectonically active area with movement currently dominated by the San Andreas Fault system, a series of right lateral strike-slip faults that separate the Pacific and North American plates. The San

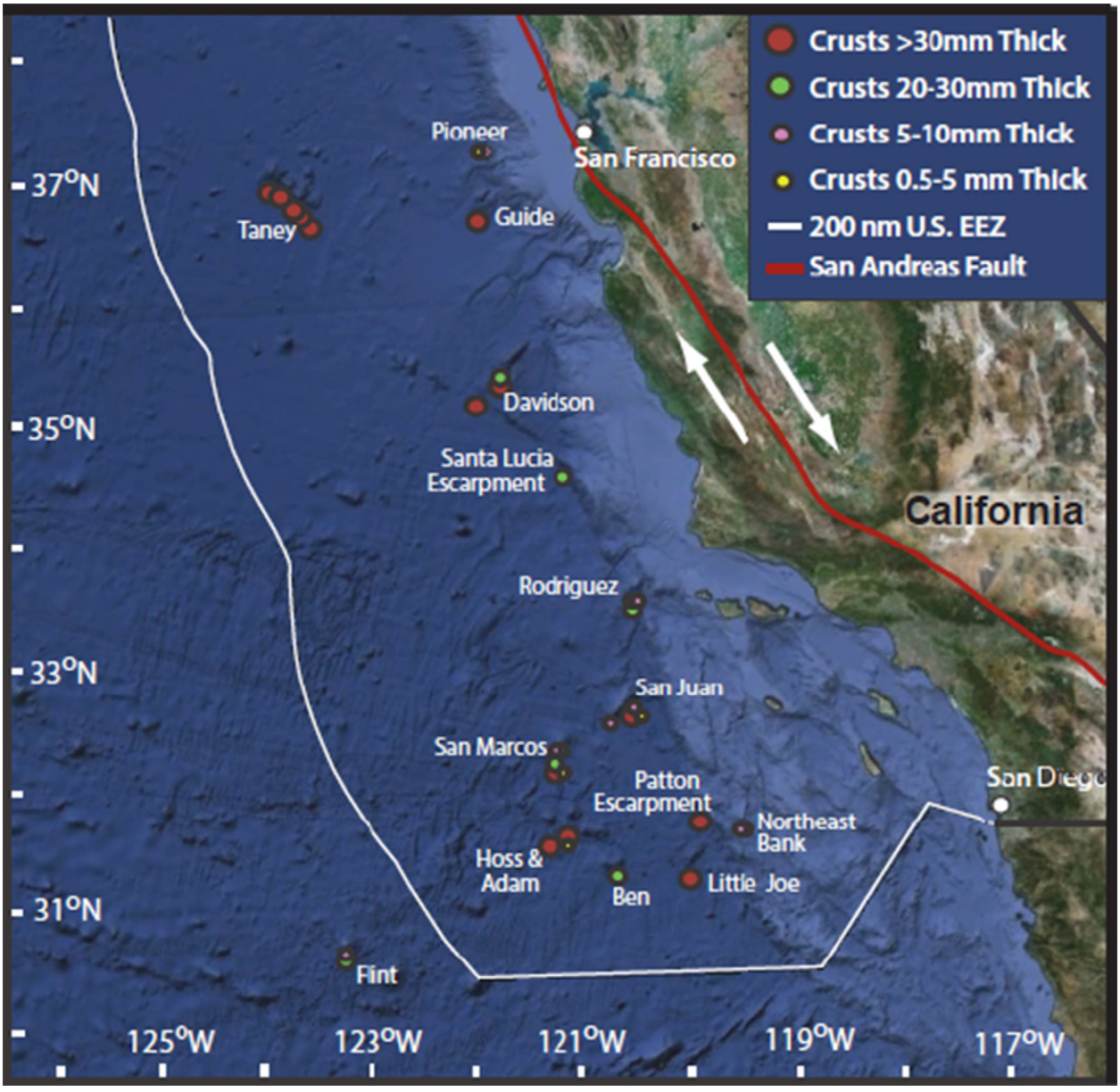

Fig. 1. Map of the sample area with seamounts labeled and mean thicknesses indicated.
(Google Earth 2015, U.S. EEZ from https://maritimeboundaries.noaa.gov/arcgis/rest/services/MaritimeBoundaries/US_Maritime_Limits_Boundaries/MapServer/3, 2/2016).

Andreas is currently moving at a rate of approximately 35 mm/yr (Powell and Weldon, 1992). The total movement northward of the Pacific Plate relative to the North American Plate is approximately 600 km over 20 Ma (Powell and Weldon, 1992). Basin and Range extension began around 17 Ma and continues today. Paleo-tectonic events include the opening of the Gulf of California between 7.7 and 5.8 Ma, and uplift of the Coast Ranges and Sierra Nevada approximately 5 Ma (Holt et al., 2000; Oskin and Stock, 2003). The oceanic crust age for the sampled region ranges from approximately 30 to 20 Ma based on magnetic anomalies (Atwater and Severinghaus, 1989; Cande and Kent, 1995; Davis et al., 2002).

The California Current System (CCS) is the eastern boundary region of the North Pacific Subtropical Gyre and exhibits strong upwelling of cold, nutrient-rich water with upwelling velocities between 10 and 20 m d^{-1} during the spring and summer seasons due to northwesterly winds and Ekman transport (Biller and Bruland, 2013; Carr, 2001; Checkley and Barth, 2009). Increasing element concentrations along the path of deep-water circulation are controlled by biogeochemical cycles and residence times and enrichment from continental margin sediments to the benthic boundary layer. Upwelled water contains high concentrations of macronutrients (nitrate, phosphate, silicic acid) and micronutrients (Fe, Mn, Co, Ni, Cu, Zn, Cd) promoting phytoplankton growth (Biller and Bruland, 2013). The upwelled water is transported off shore and nutrient distributions are affected by mixing, biologic drawdown, and particulate scavenging (Biller and Bruland, 2013).

The dominant water masses along the CCM are the North Pacific Intermediate Water (NPIW) (~300–600 m), Antarctic Intermediate Water mixed with NPIW (~600–1300 m), Pacific Deep Water mixed with Upper Circumpolar Deep Water (~1300–3800 m), and Lower Circumpolar deep Water (below 3800 m) (Conway and John, 2015; Talley, 2008). A pronounced OMZ is present in waters of the CCM, the depth of which varies seasonally but averages ~550–2000 m with oxygen concentrations <75 nmol kg^{-1} (Conway and John, 2015).

Seamounts and escarpments along the CCM are primarily composed of basalt and frequently show pillow structures. Edifice summits range from 516 m (NE Bank) to over 3700 m (Taney D) (Supplemental Table S1). The basement age for the sample region ranges from ~30 to 20 Ma based on magnetic stratigraphy with seamounts ranging in age from ~20 to 7 Ma (Atwater and Severinghaus, 1989; Cande and Kent, 1995; Davis et al., 2002).

The Taney Seamount chain consists of five submarine volcanoes (A through E from north to south) and is 53 km long (Clague et al., 2000; Coumans et al., 2015). Remotely operated vehicle (ROV) and dredge samples collected from Taney Seamounts consist of enriched mid-ocean ridge basalt and slightly alkalic and tholeiitic (Taney A) basalts and have high Al_2O_3 and low SiO_2 contents; with some pillow structures indicating emplacement in a submarine environment (Clague et al., 2000; Coumans et al., 2015). Submarine imaging surveys found little sediment accumulation, making the Taney Seamounts an ideal location for Fe-Mn crust formation (Clague et al., 2000). The Taney Seamount chain has several edifices with very flat tops resulting from caldera collapse and infilling of earlier large calderas, rather than wave erosion from subsidence after subaerial exposure (Clague et al., 2000; Coumans et al., 2015).

Pioneer, Gumdrop, Guide, and Davidson Seamounts are composed of similar rock types, ranging from alkalic basalts to trachyte and have the northeast-southwest orientation that is common in this region (Davis et al., 2002, 2010). These seamounts consist of a series of parallel ridges and aligned cones separated by sediment filled troughs and lack summit craters or calderas (Davis et al., 2002). The most common rocks on all of these seamounts are alkali basalt, hawaiite, and mugearite (Davis et al., 2002). Davidson and Guide Seamounts formed above a fossil spreading center and Davidson is intersected at its southwest end by a fossil transform fault, the Morro Fracture Zone (Clague et al., 2009; Davis et al., 2002, 2010). Davidson Seamount is part of the Monterey Bay National Marine Sanctuary and is considered a pristine habitat for a variety of species including deep sea corals.

Rodriguez, San Juan, and North East Bank all have features consistent with subaerial exposure including graded sand, gravel, and cobble beds (Paduan et al., 2009). They also have volcanic glass with lower sulfur concentrations than found on other CCM seamounts; this is consistent with subaerial degassing of the lava (Paduan et al., 2009). Lavas from the summits of these three seamounts do not have pillow structures or glassy rinds, which also indicate subaerial flows (Paduan et al., 2009). The shallowest pillow structures on Rodriguez, San Juan, and North East Bank were found at 925, 1282, and 560 m below sea level respectively (Paduan et al., 2009). These seamounts are thought to have subsided due to thermal contraction of the oceanic crust from 11 to 7 Ma (Paduan et al., 2009). Based on the modern water depths of the seamount summits and the extent of terrestrial deposits, Paduan et al. (2009) proposed that Rodriguez and San Juan subsided approximately 700 m while North East Bank subsided 500 m since their formation.

The Patton Escarpment is a relict accretionary wedge that lies at the edge of the continental shelf (Marsaglia et al., 2006). It is thought that a trench-ridge-trench triple junction was present at the Patton Escarpment 18 to 16 Ma (Marsaglia et al., 2006). The Santa Lucia Escarpment lies near the intersection of the continental shelf and the Morro Fracture Zone, south-east of Davidson Seamount (Gibbs et al., 1993). Spreading centers were active near the Santa Lucia Escarpment in the early Miocene (Gibbs et al., 1993).

Adam and Hoss Seamounts are small adjacent edifices with Fe-Mn encrustations on most dredge samples recovered. On USGS cruise F7-87-SC, fewer than 15% of samples collected by dredging on San Marcos Seamount were coated with Fe-Mn crusts (Hein et al., 2010b). All of the samples collected from Little Joe had some Fe-Mn encrustation, most of moderate thickness, from 10 to 35 mm, with some crusts up to 65 mm thick (Hein et al., 2010b). Ben Seamount has little sediment cover, but sediment deposits exist next to the north flank (Hein et al., 2010b).

3. Methods

Fe-Mn crust samples were selected for chemical analysis based on location. A range of water depths and sample thicknesses were selected to represent the different sites, if possible. Samples influenced by hydrothermal inputs, identifiable by chemical signatures, were excluded. Hydrogenetic samples are considered to be those with Fe/Mn ratios between 0.5 and 3.0 (Hein et al., 1993). The concentrations of minor elements were also considered in sample selection; samples with Co, Ni, and Cu concentrations multiplied by 10 that are less than 5% are considered to be hydrothermal based on the traditional discrimination ternary diagram (Bonatti et al., 1972; Hein et al., 1993) and excluded from comparisons.

Chemical analyses of major and minor elements in the crusts were performed by SGS Canada analytical laboratory. Analyses of major elements were run using borate-fused disk X-ray florescence as oxides. Minor elements were analyzed by inductively coupled plasma mass spectrometry (ICP-MS) after a 4-acid (HCl, HF, HNO_3, and $HClO_4$) digest, the resulting solution was dried and dissolved in 1 ml aqua regia and diluted to 10 g with 1% HNO_3. Rare earth elements plus yttrium (REY) were analyzed using Li-metaborate fused disk dissolved in weak HNO_3 and analyzed by ICP-MS. Tellurium and Se concentrations were determined following the same 4-acid digest and hydride generation with a modified flow-injection and analyzed using atomic absorption spectroscopy. Analytical precision is 1.5% or better for all elements. Sorbed (hygroscopic) water was measured by heating the sample to 110 °C for one hour and calculating the difference in wet vs dry sample weight to determine the water weight. Samples were measured dry within 10 min of removal from oven. Platinum group elements (PGE) were analyzed by Intertek Genalysis, Australia, using nickel sulfide fire assay and run on an ICP-MS with analytical precision better than 10%. Procedural blanks are less than 1 ppb for Au, Ru, Rh, Pd, Re, and Pt, 0.1 ppb for Ir,

and 3 ppb for Os. Chemical data are water normalized to 0% hygroscopic water (0% H_2O^-) so that minor elements can be more accurately compared. This is consistent with open-ocean data reported previously (Hein and Koschinsky, 2014).

Selected crusts were split into layers based on visually distinct textural or compositional differences. Compositional differences were identified based on color variations reflecting greater Mn (black) or Fe (red-brown) layers. All depths within Fe-Mn crusts are provided in mm from the top of the crust (the surface that was in contact with seawater).

The age and growth rates of Fe-Mn crusts were calculated using the cobalt chronometer, an empirically derived formula where growth rate (GR) = $0.68 / (Co^n)^{1.67}$, $Co^n = Co \times (50 / Fe + Mn)$, with metals in wt.% (Manheim and Lane-Bostwick, 1988). The growth rate model assumes a constant flux of Co into the crusts of at least one order of magnitude over the growth rate (Halbach et al., 1983). This formula does not account for growth hiatuses, erosional or dissolution events, and is considered a minimum age estimate (Klemm et al., 2005). It is also not possible to exclude changes in growth rate within a bulk sample or on a scale finer than the chemically analyzed layers.

Mineralogical compositions were determined by X-ray diffraction (XRD) using a Philips diffractometer with Cu Kα radiation and a graphite monochromator. PANalytical software packages and inorganic minerals data base were used to interpret the XRD spectra.

Plots of REY were normalized to Post-Archean Australian Shale (PAAS) values (Bau, 1996; Bau et al., 2014; McLennan, 1989). Discrimination plots used PAAS normalized REY data with $Ce_{sn}^* = 0.5La_{sn} + 0.5Pr_{sn}$ or if Pr data were unavailable $Ce^* = 0.67La + 0.33Nd$; plots are Ce_{sn}/Ce_{sn}^* vs Nd and Ce_{sn}/Ce_{sn}^* vs Y_{sn}/Ho_{sn} (Bau et al., 2014) to further confirm that the samples used for comparison are hydrogenetic. This plot did not exclude any additional samples.

The Pearson product correlation coefficient was used to calculate correlation coefficient matrices for the chemical data. The presented matrix included 141 bulk and 17 mean bulk crust samples, collected by ROV on MBARI cruises for which exact location and water depths are known (Supplemental Table S2). Mean bulk samples are the weighted percent averages of two to five continuous layers collected through a crust. The 158 samples used for the correlation matrix were also used in a Q-mode factor analysis to determine groupings of elements (Hein et al., 2012; Klovan and Imbrie, 1971). Q-mode factor analysis calculations were run in MatLab (Pisias et al., 2013). These groupings (factors) are interpreted so that each factor represents a particular mineral or mineral group in which elements associated with the factor are contained. This interpretation uses the mineralogy data and element correlations linking the mineralogy related to environmental conditions to element concentrations that represent sources.

4. Results

4.1. Samples

Samples from USGS cruises F7-87-SC and F6-87-NC were collected by chain-bag dredge and have only approximate water depths based on the length of the dredge line, tensiometer readings, and wire angle. Samples collected on MBARI cruises were obtained by ROV and have precise water depths and locations. Samples collected on the MBARI 2003, 2004, and 2010 cruises have accompanying seawater data, such as oxygen probe measurements. Unpublished water-normalized bulk and mean bulk crust data used in this study are presented in Supplemental Table S3 and statistics of the data by seamount are presented in Supplemental Table S4.

Over the entire study area, water depths of samples ranged from 570.5 m (Patton Escarpment) to 3934 m (Taney D). Water depth ranges on individual seamounts are much more limited (Supplemental Table S1). A wide range of crust thicknesses was observed ranging from a very thin <0.1 mm patina to 84 mm. Surface textures are variable and include large botryoids, microbotryoids, granular to micro-granular (dendritic), with abraded and polished areas on some of the crust surfaces. The microbotryoidal to granular surface texture was the most common. Thick CCM Fe-Mn crusts can be massive, laminar, columnar, or botryoidal laminar. Some of the thick crusts contain visually distinct layers while others do not. Thin dendritic layers also occur in some of the crust samples. Detrital grains generally from fine silt to course sand size, including some embedded cobbles are present in some of the CCM Fe-Mn crust samples, particularly those close to shore. Many of the Fe-Mn crusts had encrusted worm tubes on their upper surface with a few also having sea sponge encrustations. A few hydrogenetic seamount nodules were also found on Santa Lucia Escarpment and Adam seamount.

4.2. Mineralogy

XRD analysis of CCM Fe-Mn crusts show δ-MnO_2 to be the dominant mineral along with an X-ray amorphous FeO(OH) which crystallized to goethite in about 9% of the crusts (Supplemental Table S7; Hein et al., 2010b). While δ-MnO_2 is common in open-ocean crusts, goethite is less common and has been recorded in the oldest sections of only 6% of open-ocean Pacific crusts (Hein et al., 2000). Todorokite is present in approximately 35% of CCM Fe-Mn crusts and is slightly more common in the southern section of the sample region. Birnessite is present in approximately 5% of CCM samples; this is significant as todorokite and birnessite occur in less than 2% of open-ocean crusts if all CCM crust are excluded (Hein et al., 2000, 2010b). Detrital quartz, plagioclase, and K-feldspar are common minor minerals, and phillipsite, smectite, and illite are present in some samples. Some CCM crust samples, particularly those with very high Ba, contain minor barite. Carbonate-fluorapatite (CFA) was not detected in the CCM crusts (Supplemental Table S7; Hein et al., 2010b).

4.3. Chemistry

One hundred and fifty-five bulk Fe-Mn crust samples and 22 mean bulk samples (compiled as weighted averages from layer data) were analyzed for major and minor elements and REY (Supplemental Table S3). Layers with 2–4 subsamples per curst were also analyzed for 32 Fe-Mn crusts totaling 74 subsamples (Supplemental Table S5). Surface scrapes of the upper 0.5 to 1 mm were analyzed for an additional 63 samples (Supplemental Table S6). When a bulk crust has a thickness of 1 mm or less it was reported in the bulk data table and not in the surface scrape table. In crusts where a surface scrape was used for the upper layer of a sample, that subsample is recorded in both the layer and the surface scrape data tables with a note added in the layer table; this occurs for 6 crusts. The new bulk and mean bulk data were added to the published data from Hein et al. (2010a,b) and Gibbs et al. (1993) to calculate the CCM mean for comparison to open-ocean samples (Table 1) and to determine statistics for each seamount (Supplemental Table S4). All data are presented on a hygroscopic water-free basis (0% H_2O^-).

4.4. Comparison to open-ocean Fe-Mn crust chemistry

When comparing bulk and mean bulk CCM Fe-Mn crusts to open-ocean crusts, Si is enriched in CCM crusts with an average concentration of 10.8% (n = 225) compared to 5.21% (n = 43), 6.82% (n = 23), and 4.05% (n = 303) for Atlantic Ocean, Indian Ocean, and PCZ crusts, respectively (Table 1). The Si/Al ratio is also higher for CCM Fe-Mn crusts (6.18) than in Fe-Mn crust samples from open-ocean locations; the PCZ has the second highest Si/Al ratio (4.00). Elements typically hosted in the aluminosilicate phase of crusts, K and Na are also higher in CCM Fe-Mn crusts (0.85%, 1.97%, respectively, n = 225) compared to PCZ crusts, 0.55% and 1.64%, respectively (n = 303). The Indian Ocean crusts average 0.63% K (n = 23). The mean K and Na concentrations in CCM

Table 1
Compiled mean composition of Fe-Mn crusts and nodules from the global ocean modified from Hein et al. (2000) and Hein and Koschinsky (2014); CCM updated with data presented in this paper.

	Atlantic Ocean		Indian Ocean		Prime Crust Zone		South Pacific Ocean		CA margin		CCZ nodules	
Element	Mean	N	Mean	N	Mean	N	Mean	N	Mean	N	Mean	N
Fe (wt.%)	20.9	43	22.3	23	16.9	362	18.1	286	23.8	225	6.16	66
Mn	14.5	43	17.0	23	22.8	362	21.7	321	19.5	225	28.4	66
Fe/Mn	1.44	43	1.31	23	0.74	362	0.83	286	1.33	225	–	0
Si	5.21	43	6.82	23	4.05	303	4.75	255	10.8	225	6.55	12
Al	2.20	43	1.83	23	1.01	351	1.28	241	1.79	225	2.36	65
Si/Al	2.37	43	3.73	23	4.00	303	3.72	241	6.18	225	–	0
Mg	1.58	43	1.25	23	1.10	328	1.32	192	1.26	225	1.89	66
Ca	4.03	43	2.27	23	4.03	328	3.53	256	2.25	225	1.70	66
Na	1.26	43	1.55	23	1.64	303	1.52	88	1.97	225	1.99	66
K	0.54	43	0.63	23	0.55	303	0.63	156	0.85	225	0.99	66
Ti	0.92	43	0.88	23	1.16	345	1.12	230	0.67	225	0.32	66
P	0.75	43	0.38	23	0.96	328	0.78	265	0.57	225	0.21	66
Cl	>0.74	31	>1.00	19	0.92	43	>1.08	40	0.74	14	0.27	12
LOI	26.0	43	26.6	23	32.0	185	18.5	55	16.4	172	26.5	12
H_2O^-	10.6	43	14.1	23	19.5	303	19.8	53	18.3	224	11.6	12
H_2O^+	–	0	–	0	7.99	263	10.2	7	–	0	8.80	7
CO_2	–	0	–	0	0.74	263	0.83	7	–	0	–	0
S_T	0.25	31	0.15	9	0.26	43	0.12	40	0.01	40	0.17	12
Ag (ppm)	0.20	18	0.37	9	–	0	0.97	13	0.90	169	0.17	12
As	308	42	207	19	393	328	287	84	257	225	67	12
B (ppm)	257	13	287	10	178	43	197	40	235	13	–	0
Ba	1556	43	1533	23	1934	328	1705	143	1838	225	3500	66
Be	8.98	43	6.93	23	6.07	43	5.38	59	3.99	181	1.9	12
Bi	19.3	38	30.2	22	42.9	34	22.4	46	16.2	182	8.8	12
Br	36.5	10	54.0	6	28.1	34	29.5	72	34.3	14	–	–
Cd	4.07	34	3.47	18	3.59	285	4.14	62	3.70	223	16	12
Co	3608	43	3291	23	6662	362	6167	321	3131	223	2098	66
Cr	46.8	40	22.3	18	27.9	272	35.0	79	51.9	225	17	12
Cs	–	0	5.00	1	3.71	1	1.90	18	0.66	155	1.5	61
Cu	861	43	1105	23	976	362	1082	321	383	223	10714	66
Ga	15.5	39	16.2	23	18.8	33	28.5	27	18.2	97	36	12
Ge	0.66	18	0.64	9	0.0	0	2.40	11	0.87	149	–	0
Hf	8.71	30	9.78	15	9.43	43	9.15	81	6.12	184	4.7	66
In	0.18	19	0.26	10	0.62	1	0.87	6	0.14	170	0.27	12
Li	33.1	42	8.34	22	2.92	33	3.46	36	16.6	33	131	66
Mo	409	43	392	23	461	328	418	67	385	223	590	66
Nb (ppm)	50.9	43	61.3	23	51.6	43	59.2	46	31.5	184	22	66
Ni	2581	43	2563	23	4209	362	4643	321	2269	223	13002	66
Pb	1238	43	1371	23	1641	326	1057	113	1565	223	338	66
Rb	15.0	24	15.8	17	17.0	12	10.6	27	14.6	184	23	66
Sb	51.1	30	39.9	15	39.3	43	35.4	73	36.9	184	41	12
Sc	16.4	43	12.5	23	6.55	43	9.29	82	9.36	182	11	66
Se	0.44	10	1.73	10	14.8	1	5.06	14	2.00	175	0.72	12
Sn	8.34	28	9.68	17	10.0	10	10.91	34	4.27	171	5.3	12
Sr	1262	43	1201	23	1510	303	1483	67	1302	202	645	66
Ta	1.34	17	0.91	10	2.36	2	1.23	47	0.59	176	0.33	66
Te	43	37	31	22	60	43	38	38	13	184	3.6	66
Tl	104	38	95.4	22	155	34	154	46	49	182	199	12
Th	52	42	56	18	11	40	15	67	48	177	15	66
U	10.9	35	10.3	18	12.4	38	12.0	67	11.7	177	4.2	66
V	849	43	634	23	641	328	660	177	628	223	445	66
W	79	35	80	18	89	36	97	56	66	184	62	66
Y	181	43	178	23	221	294	177	49	172	223	96	66
Zn	614	43	531	23	668	325	698	181	554	223	1366	66
Zr	362	38	535	22	548	43	754	46	464	184	307	66
La	272	42	290	21	339	83	204	75	270	187	114	66
Ce	1392	42	1469	21	1322	83	818	75	1264	223	284	66
Pr	63.8	20	66.2	12	61.3	83	40.8	31	60.3	187	33.4	66
Nd	243	42	259	21	258	83	184	67	253	187	140	66
Sm	55.5	20	60.8	12	51.5	83	38.1	67	53.5	187	34	66
Eu	11.5	42	12.5	21	12.5	83	17.5	75	12.7	187	8.03	66
Gd	57.9	20	67.2	12	56.2	83	43.9	31	55.5	187	31.8	66
Tb	9.17	20	9.99	12	8.79	82	5.98	53	8.92	187	4.98	66
Dy	47.1	20	55.6	12	60.0	83	40.7	30	49.6	187	28.5	66
Ho	9.61	41	10.6	13	10.9	82	8.45	17	10.0	187	5.35	66
Er	28.0	20	29.3	12	31.0	83	26.5	31	27.9	187	14.6	66
Tm	3.91	20	4.03	12	4.55	82	3.6	17	3.9	187	2.11	66
Yb	23.9	42	24.8	21	28.5	83	21.9	75	25.3	187	13.7	66
Lu	3.74	20	4.05	12	4.29	40	3.33	75	3.81	186	2.05	66
Au (ppb)	5.99	2	20.7	2	99.7	7	33.1	38	7.8	17	4.5	9
Hg	85.9	37	37.8	18	9.28	12	31.8	33	11.4	161	18	3

(continued on next page)

Table 1 (*continued*)

	Atlantic Ocean		Indian Ocean		Prime Crust Zone		South Pacific Ocean		CA margin		CCZ nodules	
Element	Mean	N	Mean	N	Mean	N	Mean	N	Mean	N	Mean	N
Ir	4.8	2	6.8	5	13	56	2.5	3	1.8	9	2	11
Os	2.4	1	4.0	3	2.4	4	2.5	1	3.5	11	–	0
Pd	6.0	2	15	6	3.8	54	7.0	14	4.1	28	8	12
Pt	567	2	211	6	470	60	465	15	70	30	128	12
Rh	37	2	20	6	23	59	33	15	6	29	9	12
Ru	18	2	20	6	17	58	13	6	9	15	12	12

Fe-Mn crusts approximate those of the Clarion Clipperton Zone (CCZ) nodules at 0.99 (n = 66) and 1.99% (n = 66), respectively. Rubidium is also hosted in the aluminosilicate minerals but has a slightly lower concentration in CCM crusts with a mean of 14.6 ppm (n = 184) compared to 15.0 ppm (n = 24), 15.8 ppm (n = 17), 17.0 ppm (n = 12) for the Atlantic Ocean, Indian Ocean, PCZ respectively.

Iron is enriched in CCM Fe-Mn crusts relative to open-ocean samples with a mean concentration of 23.8% (n = 225), which is 1.5% (n = 23) greater than Indian Ocean crusts which have the second highest concentration and 6.9% (n = 362) more than PCZ crusts which have the lowest mean concentration. Iron enrichment is also apparent in the ternary diagram where the plotted bulk CCM data trend towards Fe from the hydrogenetic field defined by open-ocean Fe-Mn crust samples (Fig. 2). The mean Mn concentration in CCM Fe-Mn crusts 19.5% (n = 225) is slightly lower than in crusts from the PCZ 22.8% (n = 362) and S. Pacific 21.7% (n = 321), and slightly higher than in crusts from the Atlantic 14.5 (n = 43) and Indian 17.0 (n = 23) Oceans. The mean Fe/Mn ratio is higher in CCM crusts 1.33 (n = 225) than in the PCZ 0.74 (n = 362) and S. Pacific 0.83 (n = 286), and is more comparable to the Fe/Mn ratios of the Atlantic and Indian Ocean crusts, 1.44 (n = 43) and 1.31 (n = 23), respectively (Hein and Koschinsky, 2014).

Thorium has a higher mean concentration in CCM crusts 48 ppm (n = 177) than in PCZ or S. Pacific Fe-Mn crusts which have concentrations of 11 ppm (n = 40) and 15 ppm (n = 67) respectively. Like Fe, the mean Th concentration in CCM Fe-Mn crusts is more comparable to the Indian and Atlantic Fe-Mn crust means, 56 ppm (n = 18) and 52 ppm (n = 42) respectively. Chromium is enriched in CCM Fe-Mn crusts 52 ppm (n = 225) compared to open-ocean samples: 47 (n = 40), 22 ppm (n = 18), 28 ppm (n = 272) for the Atlantic, Indian, and PCZ, respectively.

Other elements of potential economic interest in Fe-Mn crusts including Te, Co, Cu, Mo, Ni, W, and Pt, all have a lower mean concentration in CCM Fe-Mn crusts than in open-ocean Fe-Mn crusts from all of the other study regions. Tellurium has a significantly lower mean concentration of 13 ppm (n = 184) in CCM crusts while the Atlantic Ocean, Indian Ocean, PCZ, and S. Pacific have mean concentrations of 43 ppm (n = 37), 31 ppm (n = 22), 60 ppm (n = 43), 38 ppm (n = 38), respectively. Cobalt has a mean concentration of 3131 ppm (n = 223) in CCM crusts with the second lowest mean concentration occurring in Indian Ocean crusts, 3291 ppm (n = 23), while the PCZ has the highest, 6662 ppm (n = 362). Copper in CCM Fe-Mn crusts has a mean of 383 ppm (n = 223) with the next lowest in Atlantic Ocean crusts, 861 ppm (n = 43) and the highest in Indian Ocean crusts 1105 (n = 23). Platinum has significantly lower mean concentrations in CCM crusts, 70 ppb (n = 30), with 567 (n = 2), 211 (n = 6), 470 (n = 60), and 465 (n = 15) for the Atlantic Ocean, Indian Ocean, PCZ, and S. Pacific crusts, respectively.

4.5. Rare-earth elements in CCM Fe-Mn crusts

Hydrogenetic Fe-Mn crusts from the CCM have concentrations of REY comparable to open-ocean Fe-Mn crusts for both light (La, Ce, Pr, Nd, Sm) and heavy (Eu, Gd, Tb, Dy, Y, Ho, Er, Tm, Yb, Lu) REY. Plots of

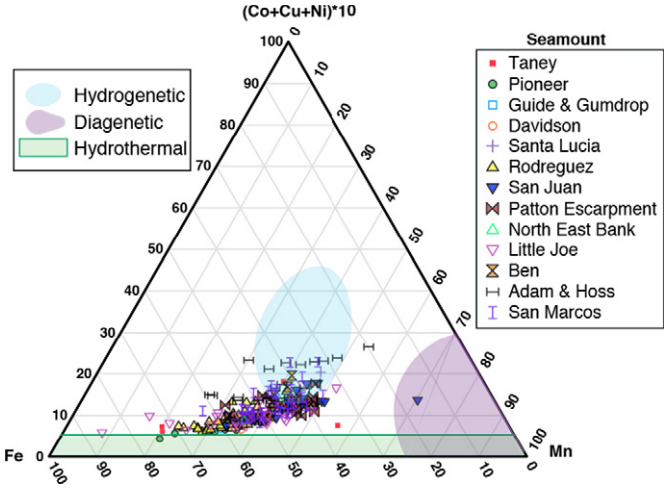

Fig. 2. Ternary diagram showing the criteria for exclusion of crust samples with samples plotted by seamount. The bottom, outlined region demarcates the hydrothermal region, the shaded Mn corner is the diagenetic field, and the light oval is the open-ocean hydrogenetic crust field (n = 300). California continental crusts trend from the hydrogenetic region towards Fe enrichment (Bonatti et al., 1972; Hein et al., 1993).

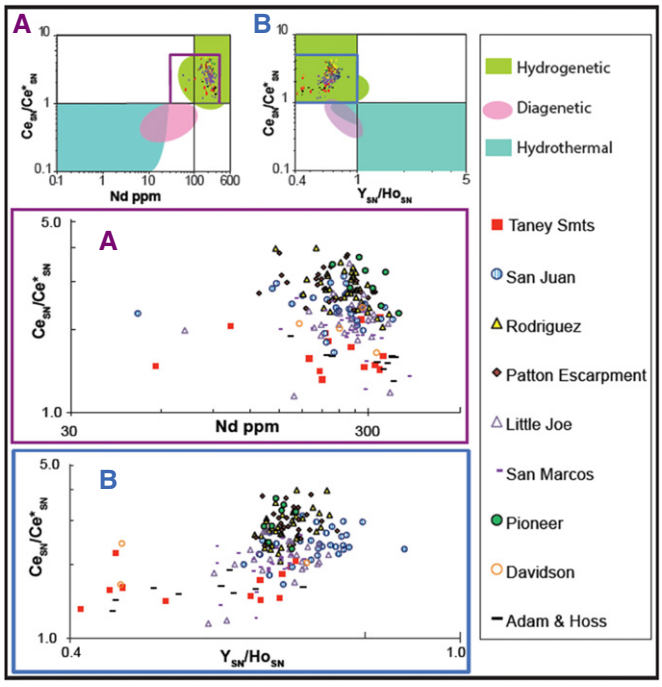

Fig. 3. Rare earth element discrimination plots after Bau et al. (2014). California continental margin Fe-Mn crusts plot in the hydrogenetic field.

the CCM Fe-Mn crust REY data normalized to PAAS are consistent with typical hydrogenetic Fe-Mn crust plots (Bau et al., 2014; McLennan, 1989). This characteristic hydrogenetic pattern shows a large positive Ce and negative Y anomaly with some samples showing smaller positive anomalies for Eu, La, and Gd (Bau et al., 2014). The REY pattern can be used to differentiate between hydrothermal Mn deposits, diagenetic Fe-Mn nodules, hydrogenetic Fe-Mn nodules and crusts (Bau et al., 2014). Patterns from 191 CCM Fe-Mn crust samples with REY data are generally consistent with hydrogenetic Fe-Mn crust profiles, with one sample each from Little Joe (T668-R13A) and San Juan Seamounts (T665-R17A) less REY enriched relative to PAAS, consistent with diagenetic Fe-Mn nodules (Bau et al., 2014; Taylor and McLennan, 1985) (Supplemental Fig. S1). San Juan Fe-Mn crust sample (T665-R17A) also plots in the diagenetic region of the ternary discrimination diagram. Those samples might have a diagenetic influence from a localized seamount sediment deposit. Hydrothermal Mn samples would also be less REY enriched relative to PAAS than typical crusts, but would have a very different profile with a negative Ce anomaly and positive Y anomaly (Bau et al., 2014), which are not observed in these two samples. The CCM Fe-Mn crusts also plot in the hydrogenetic region on PAAS normalized Ce/Ce* vs Nd (ppm) and Ce/Ce* vs Y/Ho REY discrimination plots (Bau et al., 2014) (Fig. 3).

4.6. Comparison within the CCM

Santa Lucia Escarpment Fe-Mn crusts have the highest mean Si concentration 13.9% (n = 5) and Davidson Seamount crusts have the highest mean Al concentration 2.36% (n = 3). Fe-Mn crusts from Ben Seamount have the lowest mean Si and Al concentrations at 6.41% and 1.11% respectively (n = 6) (Supplemental Table S4). The Fe-Mn crust with the highest Fe concentration is T627-R7 from the Pioneer Seamount with 33.2%. Pioneer Seamount also has the highest mean Fe concentration out of the CCM seamounts at 30.2% (n = 6). The lowest mean Fe and Mn concentrations are found on the Santa Lucia Escarpment at 16.5% and 13.7% (n = 5), respectively (Supplemental Table S4). The highest mean Mn concentration is from the Patton Escarpment at 25.1% (n = 24). The crust with the lowest Fe and Mn concentration is D6-1A from San Marcos Seamount with concentrations of 10.3% and 4.40%; that crust also has the highest Si and Al concentrations out of all CCM Fe-Mn crust samples at 25.0% and 4.89%, respectively.

Element concentrations in Fe-Mn crusts from seamounts in the northern sector of the study region, Pioneer (near shore, n = 11) and Taney Seamount Chain (off shore, n = 14) were compared to seamounts from the southern end of the study region; North East Bank and Patton Escarpment (near shore, n = 24) and Adam and Hoss Seamounts (off shore, n = 25) (Fig. 1). The near shore samples have higher Fe concentrations although the trend is slightly less apparent in crusts from the southern seamounts. When comparing the near shore samples, the northern crusts from Pioneer Seamount have higher Fe concentrations than all but three of the southern samples. There is no distinct difference in Mn, Si, Al, or K concentrations between near shore and off shore or northern and southern Fe-Mn crusts. Both P and Pb show higher concentrations in near shore crusts with slightly more overlap in Pb concentrations in the southern samples (Supplemental Table S4). Thorium also shows higher concentrations in near shore crusts for the northern sample region; there is insufficient data for southern off shore samples to make a determination. Copper shows the opposite trend with near shore data clustering below 400 ppm while the off shore data ranges up to 2088 ppm; only six of the off shore crusts have concentrations below 400 ppm.

Barium concentrations show no noticeable differences with latitude for off-shore or near-shore crusts. Off-shore Fe-Mn crust samples show a wide range of Ba from 1183 to 24323 ppm. The highest concentration of 24323 ppm (D10-4A) is an outlier with the next highest concentration at 9458 (D10-6) and the third highest is 6780 (D11-11A) all from Hoss Seamount (Hein et al., 2010b). The highest Ba concentrations measured in crusts from Taney and Adam seamounts are 6367 and 5536 ppm, respectively (Supplemental Table S4). While the lowest Ba concentrations measured in crusts from off shore seamounts are 1715, 1235, and 1183 ppm for Hoss, Adam, and Taney Seamounts, respectively. The near shore samples have a narrower range of concentrations with the highest Ba concentration of 5211 ppm on the Patton Escarpment and 1299 ppm from North East Bank and lowest concentrations on those edifices of 920 ppm and 993 ppm, respectively.

Layer and surface scrape data were used to evaluate older layers from the northern seamounts compared to the youngest layers of the southern seamounts to determine if element concentrations in Fe-Mn crusts have changed as the Pacific Plate moved northward relative to the North American Plate. Off shore seamounts Taney, San Marcos, Adam, and Hoss and near shore edifices Santa Lucia Escarpment, Rodriguez Seamount, Patton Escarpment, and Little Joe Seamount were evaluated as two separate groups. Neither group showed obvious trends for Fe, Mn, Si, Al, or P. The limited number of older layer samples from the northern edifices Taney (n = 4) and Santa Lucia Escarpment (n = 5) did not provide sufficient data for robust analysis (Supplemental Table S5).

4.7. Element correlations and associations in CCM crusts

A Pearson's product correlation coefficient matrix was used to evaluate element trends in 158 bulk Fe-Mn crust samples with known water depth, latitude and longitude, and dissolved oxygen and temperature measurements at the time of collection. The most interesting statistically significant (at the 99% confidence level (CL), p = 0.01) positive correlations are: Fe: Ag, Be, Nb, Pb, Ta, Th, Zr, and all REE; Mn: Mg, Ba, Cd, Co, Cu, Ni, W, Zn, and Te; both Fe and Mn: Ca, P, Ti, Bi, U, V, and HREE not including Eu and Gd; Si and Al both correlate with Na, K, Cr, Rb, and Sc; Si also correlates with Hf while Al correlates with Zr (Supplemental Table S2). A separate correlation coefficient matrix of 160 samples shows similar correlations and included distance from the coast, age, and growth rate. Iron increases towards shore and with decreasing water depth, while Mn only increases with decreasing water depth. Phosphorus, As, Cr, Pb, V, and Ce contents also increase towards shore. In addition to Fe and Mn, Ca, Mg, P, As, Bi, Co, Cr, Mo, Pb, Te, U, V, W, and Ce contents increase with decreasing water depth. Copper contents show the opposite trend, increasing in deeper water.

Manganese in the CCM Fe-Mn crusts shows a negative correlation with latitude at the 99% CL for both the entire data set and when evaluating only near-shore samples. Many of the elements enriched in CCM Fe-Mn crusts relative to open-ocean Pacific Fe-Mn crusts including Si, Na, K, Th, and Cr have a negative correlation with Mn at the 99% CL (Supplemental Table S2). Elements with a strong positive correlation with Mn including Ni, Te, Co, Ti, Cd, Cu, Mo, Ca, and Tl have lower mean concentrations in CCM Fe-Mn crusts than Central Pacific crusts (Supplemental Table S2 and Table 1). Element correlations with Fe are less likely to predict element enrichment or depletion in CCM crusts relative to open-ocean samples. This is likely due to the distribution of Fe in all of the major Fe-Mn crust phases.

Q-mode statistical analysis was run for three factors on the same data set, which accounted for 95.2% of variance. The three factors are interpreted to be hydrogenetic Mn; detrital Si, K, Al and Fe; and more reduced Mn phases. The third factor is thought to be birnessite- and todorokite-hosted Mn due to the high correlation coefficients with Cu, Ni, and Zn but that does not completely account for the correlation with Ba, K, and Al.

4.8. Growth rates of CCM crusts

The empirical Co-chronometer of Manheim and Lane-Bostwick (1988) was used to calculate growth rates for bulk hydrogenetic CCM Fe-Mn crust samples with seamount ages used to constrain the maximum ages (Fig. 4). CCM Fe-Mn crusts show a mean growth rate for all

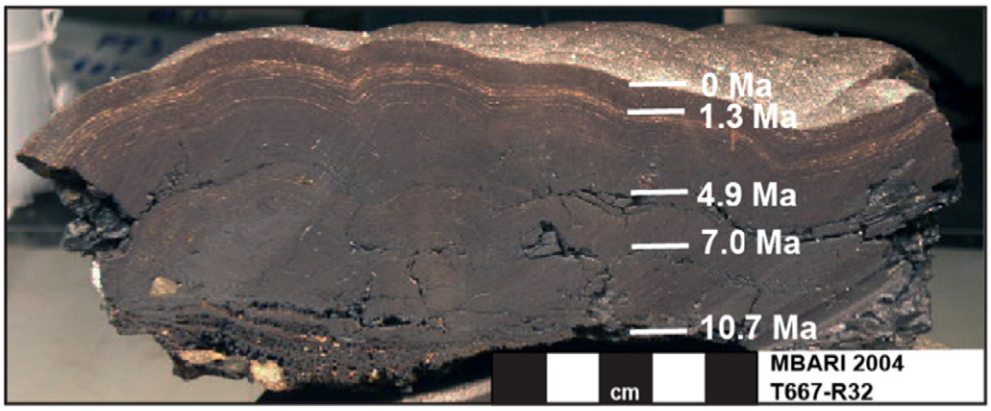

Fig. 4. Photo of hydrogenetic Fe-Mn crust T667-R32 collected from the Patton Escarpment at 1337 m water depth. White lines demark intervals sampled for stratigraphic layers with the approximate age for that depth in the crust calculated using the Co-chronometer (Manheim and Lane-Bostwick, 1988).

samples (n = 210) of 4.92 mm/Myr. The fastest growth rate is 21.9 mm/Myr from Taney D (T121-R6A). The crusts with the four fastest growth rates were all from Taney D, ranging from 17.1 to 21.9 mm/Myr with one crust from that seamount showing a more typical growth rate of 4.7 mm/Myr. Guide seamount has the next fastest growth rate of 19.7 mm/Myr (T123-R5A). Several other samples from Taney D, C, Guide, and Gumdrop have growth rates greater than 10 mm/Myr. When the seven samples with the fastest growth rates are excluded from the data set the mean growth rate drops to 4.51 mm/Myr (n = 203), all of the remaining samples have growth rates from 1 to 10 mm/Myr. This is slightly faster than growth rates for crusts from the global open-ocean, 75% of which range from 1-5 mm/Myr (Hein et al., 2000). The slowest growth rate is 1.0 mm/Myr (D17-6B) from Ben seamount. The oldest sample is from Hoss seamount (D11-11) at 27.7 Ma with the second oldest from Taney A (D176-R12) at 21.5 Ma.

A subset of 144 samples collected by ROV with exact water depth data was used to determine mean growth rate for 250 m water depth intervals and shows that growth rate increases with water depth (Fig. 5). A disproportionately large number of crust samples analyzed were collected from 1320 to 2570 m water depths.

Surface scrapes and thin bulk Fe-Mn crust samples between 0.5 and 1.0 mm thick from 67 crusts with exact water depth, temperature, and dissolved oxygen data measured in situ at the time of crust collection are used to show growth rate trends for individual seamounts (Fig. 6). Data from San Juan, Rodriguez, and combined data (all) show growth rates increasing with water depth. That trend is statistically significant at the 99% CL for San Juan and the combined data, while Rodriguez is statistically significant at the 95% CL. Little Joe, the Patton Escarpment, and Pioneer only have 6, 9, and 5 samples respectively, not enough for statistical analysis.

While growth rate does show a general increase with increasing dissolved oxygen at greater water depth that trend is only statistically significant at the 95% CL in samples from Rodriguez. Growth rate also increases with decreasing temperature, which is statistically significant for the combined data at the 99% CL and for samples from Rodriguez at the 95% CL. The difference in time scales between Fe-Mn crust growth rates and temperature and dissolved oxygen measurements must be kept in mind while evaluating trends in the data. Growth rates in this subset of data range from 1.11 to 9.13 mm/Myr and sample ages range from 0.05 Ma to 0.87 Ma, whereas O_2 and T data are for a single point in time.

5. Discussion

5.1. Mineralogy

The todorokite and birnessite present in CCM crusts could be interpreted to indicate a suboxic diagenetic input into CCM crusts. However, this interpretation is not consistent with the ternary or REY discrimination plots (Figs. 2 and 3). It is more likely that lower oxidation potential seawater conditions under which CCM crusts formed allowed for the precipitation of these Mn minerals that are less oxic than δ-MnO_2, the mineral that typifies open-ocean crusts.

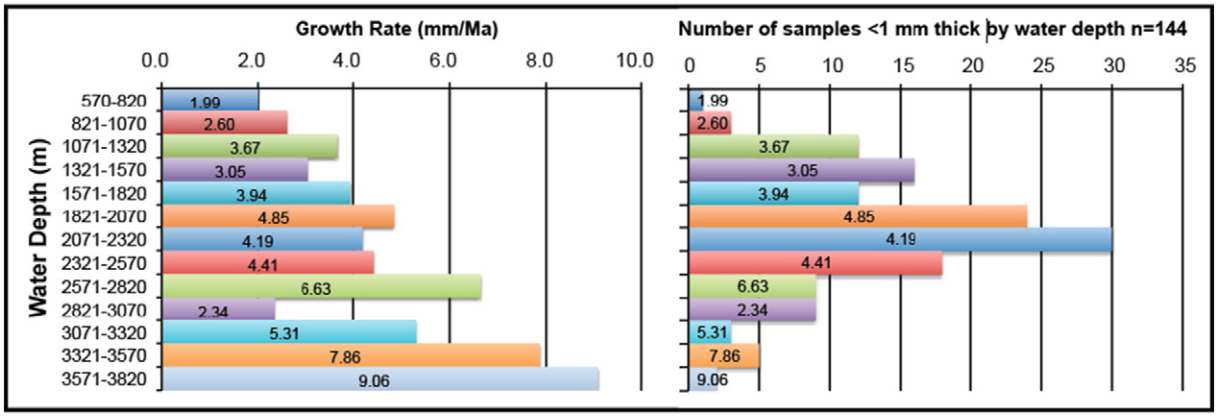

Fig. 5. Left panel: Co-chronometer growth rates and water depths for 144 California continental margin Fe-Mn crusts. Right panel: Number of samples collected at each water depth with growth rate indicated (Manheim and Lane-Bostwick, 1988).

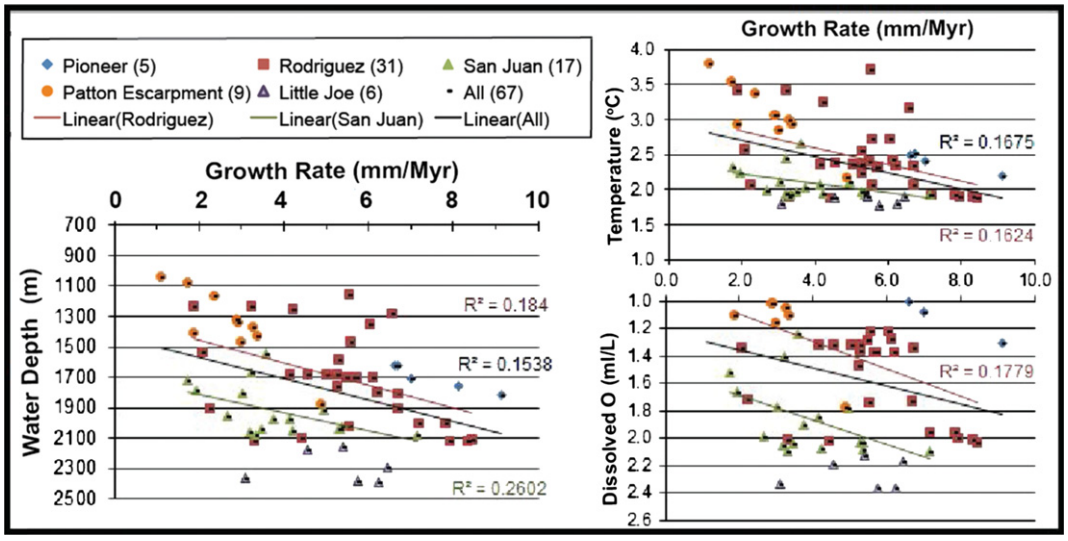

Fig. 6. Co-chronometer growth rates relative to water depth (A), dissolved oxygen (B), and temperature (C) for the upper 0.5 to 1.0 mm of 67 Fe-Mn crust samples collected by MBARI ROV.

Open-ocean Fe-Mn crusts are phosphatized by carbonate fluorapatite (CFA) impregnation of the older layers (Hein et al., 1993; Koschinsky et al., 1997). CFA deposition occurs by preferential replacement of calcium carbonate and partial replacement of Fe oxyhydroxides by CFA, and precipitation of CFA in pore space (Hein et al., 1993; Hyeong et al., 2013; Koschinsky et al., 1997; Puteanus and Halbach, 1988). In phosphatized Fe-Mn crusts Si, Fe, Al, Ti, Co, Mn, and Pb are depleted in that order with Si in particular showing up to a 45% decrease, whereas Ni, Cu, Zn, and REY are enriched, with Ni showing up to a 30% increase (Koschinsky et al., 1997). Phosphatization occurred in suboxic environments from nutrient-rich water in extended and intensified OMZs (Halbach et al., 1989; Hein et al., 1993; Koschinsky et al., 1997). Phosphate could also be supplied by upwelling into the OMZ of phosphate enriched deep water, where nutrients accumulated during stable climatic times (Hein et al., 1993). Open-ocean Fe-Mn crusts from the central Pacific show that two major phases of phosphatization occurred during climatic transitions at the Eocene/Oligocene (39–34 Ma), and the Oligocene/Miocene boundaries (27–21 Ma) (Hein et al., 1993). A minor phase of phosphatization may have occurred during the middle Miocene (Hein et al., 1993). Open-ocean Pacific crusts do not show evidence of phosphatization past the middle Miocene.

Fe-Mn crusts from CCM seamounts do not contain detectable CFA and show no evidence of phosphatization. The paucity of phosphatization in CCM Fe-Mn crusts is curious, as there are extensive formations of authigenic CFA phosphorites on the shelf, slope, and banks adjacent to CCM low-oxygen basins (Berndmeyer et al., 2012; Filippelli et al., 1994; Laurent et al., 2015). The Miocene Monterey Formation is one of the best-studied examples of CCM phosphate deposition, which outcrops along the CCM between San Francisco and Los Angeles. Phosphate occurs as a phosphate-rich carbonaceous member deposited from 14.5 to 14.1 Ma (during a period of cooling climate) and interstratified phosphatic laminae and lenses deposited from 11.05 to 7.85 Ma (Berndmeyer et al., 2012; Laurent et al., 2015). Based on the occurrence of phosphatized layers in open-ocean Fe-Mn crusts as recent as 10 Ma and phosphorite deposition in the study area along the CCM up to 7.85 Ma, the lack of phosphatization in CCM Fe-Mn crusts is unexpected. Approximately 19% of CCM bulk crusts and crust layers are older than 7.85 Ma and the older sections of those samples do not show element trends consistent with phosphatization. In addition, calcium carbonate minerals are scarce in CCM Fe-Mn crusts eliminating the possibility of phosphatization through the replacement of carbonates.

Suboxic environments have occurred around the CCM seamounts during much of their history, as evidenced by the Mn mineralogy. However, the seawater around the offshore seamounts may not have been depleted enough in oxygen and consequently enriched enough in phosphate to form CFA in these Fe-Mn crusts. Fluorine is also a necessary component in CFA but as a conservative element in seawater, F depletion sufficient to hinder CFA deposition is unlikely. More likely, primary productivity due to upwelling may not have been intense enough above the seamounts to provide the organic matter, and associated phosphorous, necessary to establish phosphatization. Despite the occurrence of the OMZ, upwelling and primary productivity were likely not intense enough to form organic matter-rich sediments leading to organic matter-poor depositional environments since the middle Miocene.

5.2. Sources and distribution of Fe and Mn

Flux of Fe and Mn were calculated for 62 Fe-Mn crust surface samples up to 1 mm thick with exact water depth and location data (Supplemental Table S6). The equation used to calculate flux is (F (μg cm^{-2} kyr^{-1}) = $C_e GrD$) where F is flux (μg cm^{-2} kyr^{-1}), C_e is the dry elemental concentration, Gr (mm/Myr) is growth rate (calculated from the cobalt chronometer), and D (1.3 g/cm^{-3}) is dry bulk density (Hein et al., 2009; Halbach et al., 1983). Since cobalt chronometer growth rates were used in the calculation Fe and Mn fluxes are not completely independent. Iron flux ranges from 31 to 575 (μg cm^{-2} kyr^{-1}), while Mn flux ranges from 47 to 285 (μg cm^{-2} kyr^{-1}). Pioneer Seamount had the largest Fe and Mn fluxes while the smallest Fe flux was from San Juan and Mn flux was from the Patton Escarpment (Supplemental Table S6). The flux of Fe in CCM Fe-Mn crusts is much greater than the Mn flux and shows greater variation, which is consistent with the complex nature of Fe in a continental-margin environment.

Terrestrial sources deliver trace metals to the surface ocean, specifically fluvial particulate matter delivered during winter precipitation is a significant source of Fe, Mn, and other trace metals to the continental shelf (Biller and Bruland, 2013). Eolian sources also contribute to the trace metal budget of the surface ocean (Mackey et al., 2002). In addition to aeolian and fluvial input of Fe into the surface waters, remobilization from shelf/slope sediments, and input of hydrothermal vents can also release Fe into intermediate and deep-water masses (Horner et al., 2015). Earth's continental crust contains more Fe (~4%) than Mn (~0.08%) (Rudnick and Gao, 2014), but has a lower Fe/Mn ratio than

the average oceanic crust (Fe/Mn 69.8) (White and Klein, 2014), mid-ocean ridge basalt (Fe/Mn = 54) (Qin and Humayun, 2008), and Hawaii ocean island basalt (Fe/Mn = 67) (Humayun, 2004). These ratios are not reflected in seawater, where Fe has a nutrient-type profile with low surface water concentrations of about 0.05 nmol Fe/L due to assimilation by primary producers in surface waters (Boyd and Ellwood, 2010). Iron is then regenerated with a maximum concentration at around 1000 m of approximately 0.7 nmol Fe/L, before being scavenged at depth with slight seawater concentration decrease (Biller and Bruland, 2013; Boyd and Ellwood, 2010; Bruland and Lohan, 2003). Conversely, Mn has a scavenged seawater profile; with higher surface water concentrations and decreasing concentrations with depth (Biller and Bruland, 2013).

Remobilization of shelf sediment provides a significant source for scavenged and hybrid type elements including Fe and Mn (Biller and Bruland, 2013). Iron is a critical trace metal used in photosynthesis and nitrate assimilation and regions along the CCM show evidence for Fe limitation (Biller et al., 2013; Morel et al., 2014). Leachable particulate and dissolved Fe along the CCS is related to both upwelling intensity and the width of continental shelf mud belts between 50-90 m isobaths (Biller et al., 2013). Leachable particulate Fe concentrations are highest in coastal areas with the widest mid-self-mud belts and with a hypoxic benthic boundary layer; this has a greater influence on Fe concentrations than the overall shelf width (Biller et al., 2013). Iron isotopes from open-ocean Pacific crust CD29-2 from 20 Myr to the present show that seawater ($\delta^{56/54}$Fe ~ +0.4‰) is offset from dust end members ($\delta^{56/54}$Fe ~ +0.7‰) by −0.3‰ (Horner et al., 2015). The secondary source of Fe is isotopically light and is likely due to reductive sediment mobilization of metals (Horner et al., 2015). Under low-oxygen conditions, such as those associated with the high primary productivity along the CCM, reduced, bioavailable, isotopically light Fe is released from shelf sediments (Horner et al., 2015). Seawater measurements have shown that isotopically light dissolved δ^{56}Fe from reduced shelf sediments is laterally transported at least 1900 km off shore from the California Margin between ~550 and 2000 m water depths in the OMZ (Conway and John, 2015).

Further support for continental shelf and slope sediments as a source of Fe can be gleaned by comparison of Fe-Mn crusts from near shore (Pioneer and Gumdrop Seamounts) and offshore (Taney Seamounts) in the northern sector, and offshore (Adam and Hoss Seamounts) and near shore (Patton Escarpment and Northeast Bank) in the southern sector shows that Fe is typically higher in samples closer to the continental margin (Supplemental Table S4). Iron is consistently higher near shore when comparing Fe-Mn crust samples off a narrower shelf in the northern sector where Fe is over 29.2% in all samples from Pioneer and Grumdrop Seamounts (n = 7) and under 20.2% from all Taney Seamount Chain crusts (n = 14). In the southern sector, Patton Escarpment and Northeast Bank (n = 27) are much closer to the coast than Adam and Hoss seamounts (n = 22) and typically have higher Fe concentrations, with a few exceptions. When comparing the northern and southern seamounts, Pioneer, the seamount closest to shore, has the highest Fe concentration. No difference in Fe concentration exists between crust samples from the Taney Seamount Chain compared to the Adam and Hoss seamounts when reviewing Fe concentrations off shore and parallel to the coastline from the northern and southern ends of the study area. This shows that Fe released from continental shelf/slope sediments is the most likely source of Fe to CCM Fe-Mn crusts, and proximity to that source accounts for the Fe enrichment in CCM Fe-Mn crusts

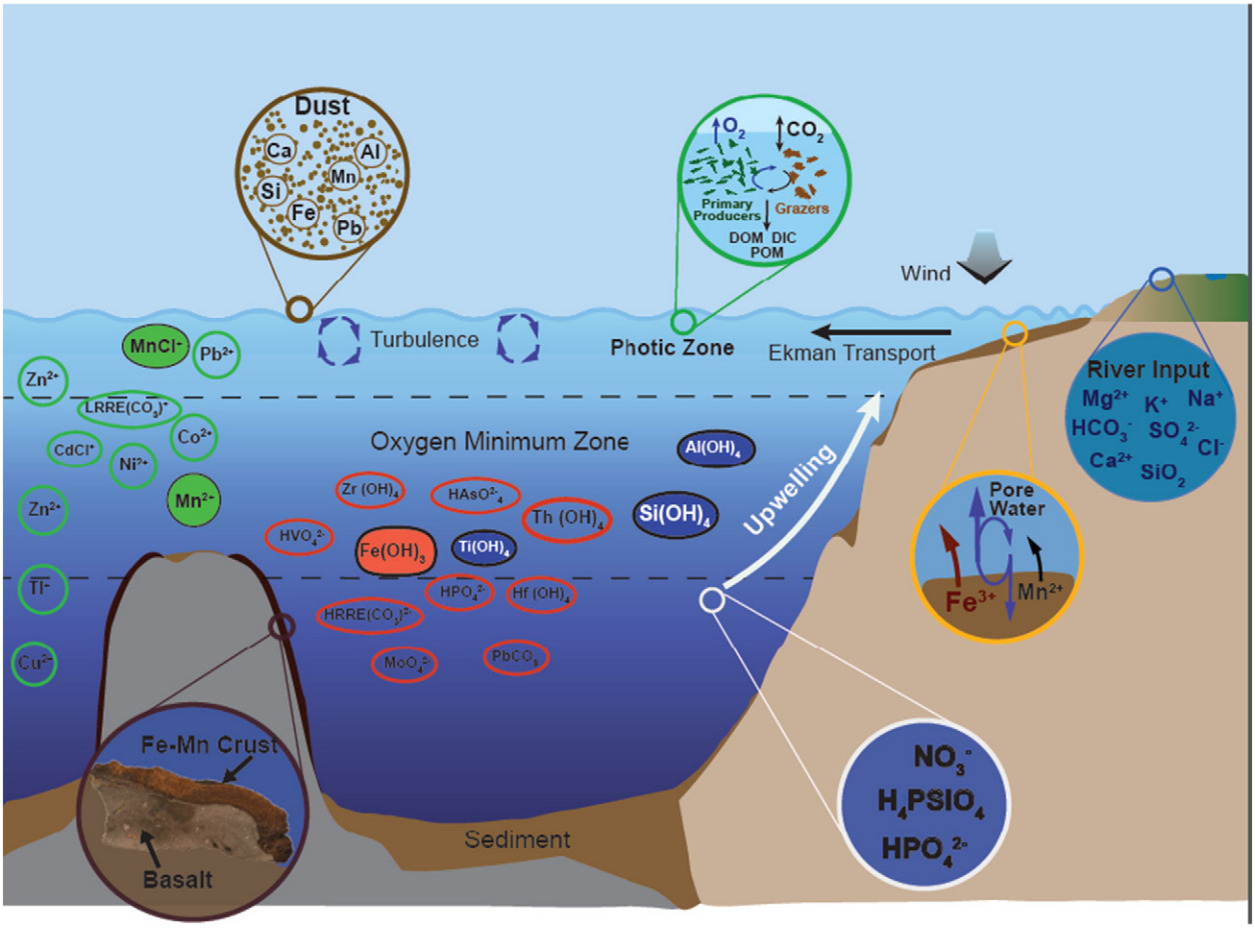

Fig. 7. Genetic model showing sources of elements into the CCM and regional influences on Fe-Mn crust formation. DOM = dissolved organic matter, DIC = dissolved inorganic carbon, POM = particulate organic matter.

relative to open-ocean crusts. A simplified genetic model showing sources and regional influences on seawater and therefore CCM Fe-Mn crusts is presented in Fig. 7.

Manganese is also influenced by these processes and reduced Mn is remobilized from shelf sediments (McManus et al., 2012). However, unlike Fe, Mn in CCM crusts does not show a concentration increase towards the continental shelf. Manganese does show a negative correlation with increasing water depth as expected since dissolved Mn is enriched in seawater in the OMZ. Mn concentrations in Fe-Mn crusts are controlled by the redox potential of seawater from which the crust formed.

5.3. 4.3 Thorium enrichment

The most common Th isotope in seawater is ^{232}Th, typically hosted by detrital material from aeolian sources; ^{232}Th has a conservative distribution in seawater down to the benthic boundary layer where there is a concentration increase (Chen et al., 1986; Hsieh et al., 2011). Dissolved and particulate ^{230}Th have profiles with a linear concentration increase with water depth and that show concentration increases along the path of circumpolar deep-water circulation (Mangini and Key, 1983; Roy-Barman et al., 1996). Decay of ^{238}U produces ^{234}Th, which has a short half-life of 24.1 days and is generally in equilibrium with its parent with a conservative seawater profile (Coale and Bruland, 1987). However, in surface water with high particulate organic carbon, ^{234}Th is scavenged and removed to the sediments at a faster rate than ^{238}U (Coale and Bruland, 1987).

Thorium is enriched in CCM Fe-Mn crusts relative to open-ocean Pacific crusts, with contents comparable to crusts from the Atlantic and Indian Oceans. The enrichment of ^{230}Th in older water masses, and increased input of ^{232}Th due to proximity to the continental margin is the most likely cause of Th enrichment in CCM Fe-Mn crusts. Dissolved Th has a residence time in seawater of <100 years because it is very particle reactive (Hein et al., 2012; Nozaki et al., 1987). Thorium positively correlates with Fe and Si and negatively correlates with Mn at the 99% CL in CCM crusts indicating that the higher Fe concentration may also help to account for the increased Th concentration observed in CCM Fe-Mn crusts relative to open-ocean crusts. Dissolution of biogenic silica is thought to be an additional seabed source for Th, as is biogenic calcite, both of which adsorb Th from the water column (Hein et al., 2012). There is also no correlation between Th and water depth in CCM crusts, unlike samples from Shatsky Rise in the NW Pacific and the Ninetyeast Ridge in the Indian Ocean where Th correlates with increasing water depth (Hein et al., 2012, 2016).

5.4. Element relationships with primary productivity

The Si/Al ratio is significantly higher in CCM crust samples, 6.2 for n = 225 relative to a mean value of 3.7 n = 610 for all other global open-ocean deposits (Hein and Koschinsky, 2014). In CCM crusts neither Si nor Al show an increase towards the continental shelf, when comparing concentrations from off shore and near shore seamounts. If the Si enrichment in CCM crusts was due to terrestrial input, or dissolved biosilica from surface water diatom primary productivity, Si contents in CCM Fe-Mn crusts would be expected to increase towards shore. Since this relationship is not found, the high Si concentrations in CCM crusts is likely due to the high Si concentrations in NE Pacific seawater. Dissolved Si in seawater ranges from 10 to 40 μmol/kg in the Atlantic, and up to 180 μmol/kg in the NE Pacific (Johnson et al., 2006; Talley and Joyce, 1992). Evidence of the high Si in the waters along the CCM area is also present in several basins along the California borderland; this is shown in the Monterey Formation, which has an increase in biosilica from ~9.3 Ma onwards (Laurent et al., 2015).

The high concentration of dissolved Si in the Pacific is due in part to the North Pacific silica plume. The North Pacific silica plume originates in the NE Pacific, extends across the North Pacific from 50°N to 20°N, and is centered around 2300 m water depth (Johnson et al., 2006; Talley and Joyce, 1992 and references therein). The maximum concentrations of Si in the plume reach approximately 164 Tmol above the average background of 165 μmol/L (Johnson et al., 2006). Possible sources of dissolved silica in the North Pacific silica plume include; hydrothermal venting, remineralization of biosilica in the water column from surface diatoms, dissolution of bottom sediments, and accumulation of bottom water silica along the path of deep water circulation (Talley and Joyce, 1992). Additionally sediment compression and thermal advection through faults during the formation of the accretionary margin might provide an additional source of Si to the region (Johnson et al., 2006).

Other trace metals, Ni, Zn, and Cd with nutrient-type seawater profiles also show enrichment in bottom-waters along the path of deep-water circulation (Bruland and Lohan, 2003). However, these elements are not noticeably enriched in CCM crusts relative to open-ocean crusts. Barium and P both have nutrient-type profiles in seawater and can be used as tracers of primary productivity (Broecker et al., 1982; Chan et al., 1976; Paytan and Griffith, 2007). However, Ba and P are also not enriched in CCM Fe-Mn crusts relative to open-ocean crusts. With the exception of a few outliers, P shows higher concentrations in near shore CCM crusts relative to off shore samples, which probably reflects the strong upwelling and primary productivity.

CCM crust samples with high Ba contain minor barite, this is observed on Hoss Seamount (D10-3 and D10-4A) and Little Joe Seamount (D13-2C) (Hein et al., 2010b). However, overall CCM Fe-Mn crusts have somewhat lower Ba concentrations than crusts from the PCZ, 1838 ppm (n = 225) and 1934 ppm (n = 328), respectively. In contrast, the CCM crusts do have higher Ba concentrations than the Fe-Mn crust mean from the Atlantic and Indian Oceans, 1556 ppm (n = 43) and 1533 ppm (n = 23), respectively. Barium in near shore CCM Fe-Mn crusts partially overlaps with the lower concentration in off shore samples. That indicates that Ba is not consistently higher in crusts closer to the shelf or continental margin.

Marine barite can form in a number of ways, for example authigenic processes occurring in sulfate reducing sediments during diagenesis, cold-seep fluids along the seafloor, low-temperature hydrothermal fluids <120 °C, intermediate-temperature fluids (150–250 °C), and precipitation in the water column typically in the presence of organic matter (Hein et al., 2007; Paytan et al., 2002). Fe-Mn crust samples with Ba concentrations significantly higher than the regional Fe-Mn crust mean may have been exposed to localized cold-seep or low temperature, diffuse-flow hydrothermal fluids, despite the overall hydrogenetic origin of the crusts.

5.5. Growth rate

Increasing growth rate with increasing water depth is an expected trend and is likely due to increasing dissolved oxygen concentrations in seawater below the oxygen minimum zone (Halbach et al., 1983; Hein et al., 2016). The correlation of Fe-Mn crust growth rate and water depth is not due to a relationship between Fe or Mn concentrations with water depth. Plots of these elements in Fe-Mn crusts versus water depth for the same data set do not show a significant correlation. The trend is also not due to continental proximity as growth rates continue to trend with water depth in Fe-Mn crusts from individual seamounts. Dissolved Mn concentrations in seawater correlates with the strength of the OMZ which provides a reservoir of dissolved Mn; with advective and diffusive transport Mn moves out of the OMZ and is oxidized (Dickens and Owen, 1994; Halbach and Puteanus, 1984; Hein et al., 2016). It is significant that CCM crusts continue to grow in a region with a well-developed OMZ, and that growth rates are slower in the OMZ than below the OMZ. This correlation has not yet been determined elsewhere in the global ocean and needs to be resolved for open-ocean settings where the OMZ is weaker. However, this does assume that the OMZ has been present since crust formation began. It also assumes that sufficient supplies of Fe and Mn, with residence times in seawater of around

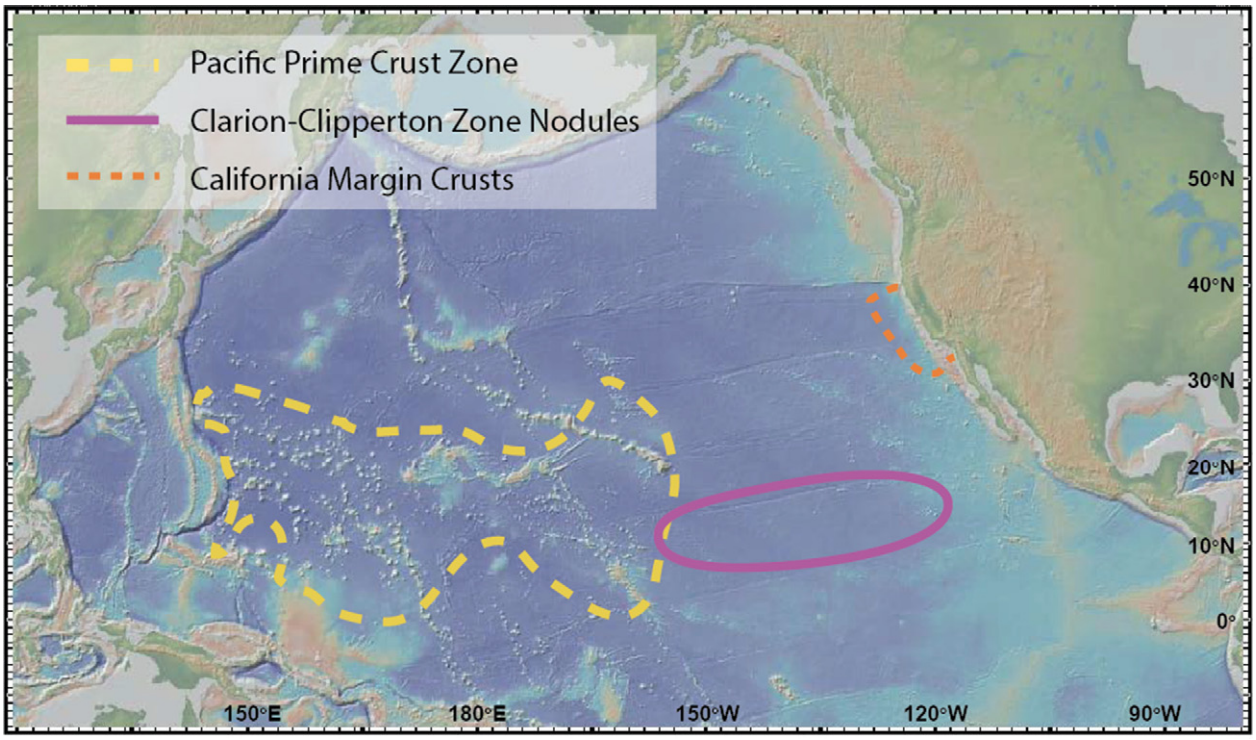

Fig. 8. Map of the North Pacific Ocean showing areas within which marine mineral samples were collected and discussed in this paper (http://www.geomapapp.org; Ryan et al., 2009). (Modified from Hein and Koschinsky, 2014).

500 years and 100 years respectively, have been available for Fe-Mn crust formation (Johnson et al., 1996, 1997). Alternatively, the increased growth rate with water depth observed in CCM Fe-Mn crusts may indicate deep-water sources of Fe and Mn influencing Fe-Mn crust formation.

5.6. Resource potential of CCM crusts

Elements of economic interest in Fe-Mn crusts include Mn, Ni, Co, Ti, Te, Th, W, Bi, REY and PGE (Hein et al., 2013). Co and

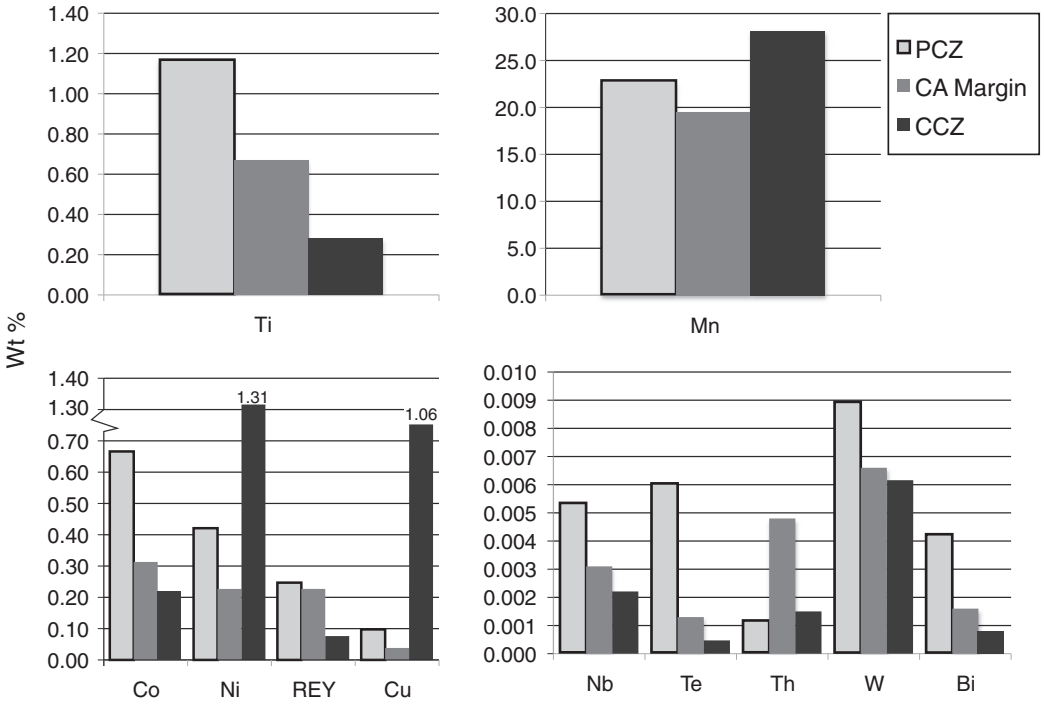

Fig. 9. Concentrations of elements of economic interest in Fe-Mn crusts from the Prime Crust Zone (PCZ) in the NW Pacific and the California continental margin and diagenetic Fe-Mn nodules from the Clarion-Clipperton Fracture Zone (CCZ) in the central-east Pacific (Hein and Koschinsky, 2014).

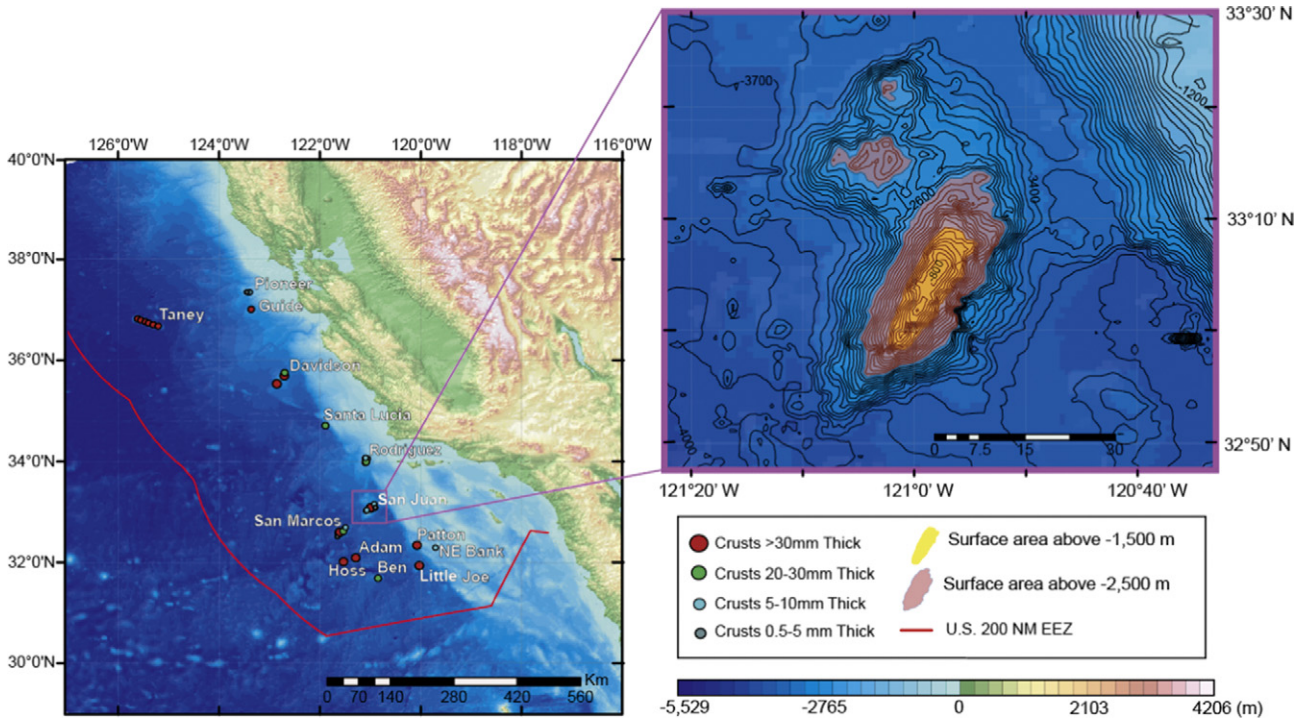

Fig. 10. Bathymetric image of San Juan Seamount showing surface area above 2500 m (white) and 1500 m (dark grey) water depths (Google Earth 2015; GEBCO, 2014; ESRI, 2011).

then Ni and Mn have traditionally been considered to have the most economic potential (Hein et al., 2013). However, increased demand for critical metals including Te and the REY may change the economic outlook of mining these deposits. There is also an increasing economic demand for Cu and while it would not be economically viable to mine crusts solely for Cu, as the grade is much lower than that of CCZ nodules and some seafloor massive sulfide deposits, the amount of Cu in crusts is of interest as a byproduct of mining (Hein et al., 2013).

The two main regions in which the most data for Fe-Mn marine minerals are available are the PCZ, which hosts hydrogenetic Fe-Mn crusts, and the CCZ, which contains diagenetic-hydrogenetic Fe-Mn nodules (Fig. 8). Other regions of the global oceans are currently being explored for both ferromanganese and non-ferromanganese deposits such as seafloor massive sulfides. Approximately 2,200,000 km^2 of seabed are under contract for marine mineral exploration and 12,000 km^2 of that area is for Fe-Mn crust exploration (Hein et al., 2013). The Council and Assembly of the International Seabed Authority passed regulations governing Fe-Mn crust exploration in July 2012 and the first contracts for the exploration of Fe-Mn crusts were granted in July of 2013 (Hein et al., 2013).

Comparison of grades between CCM crusts and PCZ crusts and CCZ nodules are presented for select elements of economic interest (Fig. 9). Cu is included although Cu grades in Fe-Mn crust samples are lower than terrestrial mines, which currently have Cu grades of approximately 0.5% for porphyry copper from which about 50% of terrestrial Cu is produced. Seafloor massive sulfide deposits have small tonnages, but Cu grades can be up to 12 wt.% (Hein et al., 2013). CCM crusts have total REY concentrations of 0.227 wt.%, with the heavy REY (HREY) complement comprising 15.5% of total REY. CCM crusts have a lower grade for total REY than the large carbonatite terrestrial mines, but a much higher percentage of HREY, which are <1% in carbonatite deposits (Hein et al., 2013). Other elements of economic interest, Mn, Ni, Co, Ti, Nb, Te, W, and Bi have slightly lower grades in CCM crusts than in crusts from the PCZ. Concentrations for Mo, Zr, and total HREY are roughly comparable between the PCZ and the CCM. Th is higher in CCM crusts than in crusts from the PCZ, but is still much lower than in terrestrial REE deposits where radioactive Th in mine waste is an environmental concern (Hein et al., 2013).

To evaluate the tonnage of elements of economic interest, total surface area above 2500 m water depth was calculated for CCM edifices using G**e**neral Bathymetric Chart of the Oceans (GEBCO) 2014 base map and ArcGIS. The total surface area was reduced to account for the Monterey Bay National Marine Sanctuary, which includes Davidson seamount and by 5% for prohibitively steep slopes, followed by 10% for sediment cover, and then 25% for biologic corridors (Hein et al., 2009). In the CCM, San Juan Seamount has the greatest surface area above 2500 m with a flat summit and low sediment cover (Fig. 10). The surface area likely to contain Fe-Mn crusts in the CCM is significantly less than that of the PCZ, which has large relatively flat plateaus and guyots (flat topped seamounts) (Table 2). Crusts in the CCM are also thinner than those of the PCZ. A mean crust thickness of 1.6 cm was used based on mean CCM sample thicknesses. The crust thickness is conservative as the majority of cruises had sampling bias that strongly favored collection of basalts with little to no crust cover. Tonnage calculations are based on an average of 1.3 g/cm^3 dry bulk density for Fe-Mn crusts (Hein et al., 2009; Hein and Koschinsky, 2014). Tonnages of dry crust for the CCM and San Juan

Table 2
Surface area calculations for CCM and San Juan Seamount and dry tonnages.

	PCZ	CCZ	CCM (total)	CCM (reduced)	San Juan (total)	San Juan (reduced)
SA (km^2) ≤2500 m	–	–	1461	681	425	273
Dry tons	7.53×10^9	2.11×10^{10}	3.04×10^7	1.54×10^7	8.85×10^6	5.67×10^6

Table 3
Dry tons of in place metals of economic interest $\times 10^6$ for the CCM and San Juan Seamount.

		Mn	Ti	Co	Ni	Cu	Mo	Zr	W	Th	Te	Total REY	HREE
CA margin	tons $\times 10^6$	301	10.3	4.83	3.50	0.60	0.59	0.72	0.10	0.07	0.02	3.50	0.31
	wt.%	19.5	0.67	0.31	0.23	0.04	0.04	0.05	0.007	0.005	0.001	0.227	0.020
San Juan Smt	tons $\times 10^6$	137	4.31	2.16	1.32	0.15	0.25	0.28	0.04	0.03	0.009	1.28	0.18
	wt.%	24.2	0.76	0.38	0.23	0.03	0.044	0.049	0.008	0.005	0.002	0.225	0.032

Seamount above 2500 m water depth are presented in Table 3. While it is more likely to be economic to exploit Fe-Mn deposits in the central Pacific than along the CCM, there are advantages to CCM Fe-Mn crusts. The absence of CFA in CCM crusts and lower concentrations of P are preferred for smelting, potentially decreasing processing costs. The proximity of CCM Fe-Mn crusts to California could also reduce transportation time and expenses.

5.7. Environmental considerations

The potential environmental impacts associated with exploitation of Fe-Mn crusts along the CCM must be considered at all steps of the evaluation process. While there is no overburden to remove when collecting Fe-Mn crusts and the risk of large-scale sediment resuspension is much lower than with Fe-Mn nodules, any form of mining impact needs to be evaluated. Selecting sites down current from preserved areas with nearby seamounts and continental slope habitats that have depth ranges comparable to those on the seamounts of interest, and preserving biologic corridors on the edifice would allow for dispersal of species to the area by current transport, stepping stones, and active dispersal that would aid in recolonization. In the CCM, the CCS and nearby continental slope should enable redistribution of species. CCM seamounts are not island habitats with highly endemic faunas but rather have species compositions similar to other regional deep-sea habitats (Rowden et al., 2010). However, the CCM is a region of high primary productivity that hosts 28 cetacean, 6 pinniped, and 2 fissiped marine mammal species, and large commercial fisheries valued at over $230 million in 2012 (Lundsten et al., 2009). Sport fishing and tourism are also significant stakeholder industries in the region. Any mining activities must weigh the economic potential against possible environmental impact and the needs of other stakeholders. As crusts contain Fe and other potentially limiting nutrients, as well as potentially toxic trace metals, the effect of even a small amount of re-suspended crust on benthic and pelagic species requires further investigation. The process of mining crusts will remove non-mobile species in the impacted area. Collecting crusts on areas previously fished by trawling, where such damage has already been inflicted would limit further reduction of these species. Since only sections on seamounts with the thickest, metal-rich crusts would be considered for extraction; mining of Fe-Mn crusts would impact a much smaller portion of a seamount than trawling fisheries.

6. Conclusions

Fe-Mn crusts along the CCM have distinct chemical and mineralogical compositions relative to open-ocean samples. A number of factors may influence the formation of CCM crusts, especially their close proximity to terrestrial sources of dissolved and particulate material transported to the ocean, remobilization of Fe and Mn from sediment on the continental shelf and slope, upwelling and high primary productivity, and older deep water masses along the CCM enriched in elements with long residence times (Fig. 7). Iron is higher in CCM Fe-Mn crusts than in those from the open ocean, resulting in a higher Fe/Mn ratio. The Fe enrichment is due to the remobilization of continental shelf and slope sediments. The CCM Fe-Mn crusts show increasing Fe concentrations with proximity to the continental shelf. Thorium is also enriched in CCM Fe-Mn crusts compared to samples from the PCZ and S. Pacific, with values approaching concentrations of crusts from the Atlantic and Indian Oceans. The enrichment of Th in CCM crusts may reflect proximity to the continental shelf, aeolian sources, and the dissolution of biogenic Si. Further work is needed to determine the most prominent source.

Silica is significantly higher in CCM Fe-Mn crusts than in open-ocean samples as is the Si/Al ratio. This is likely due to the high Si concentrations in the North Pacific silica plume. Enrichment of Si in bottom waters along the path of deep-water circulation, also contributes to the high seawater concentrations of Si along the CCM. Phosphorous is another element associated with primary productivity but is not enriched in CCM Fe-Mn crusts. CCM crusts do not contain CFA or show evidence of phosphatization, which may explain why P concentrations are lower than in crusts from the central Pacific, many of which are phosphatized in the older layers. Todorokite, which is only found in 2% open-ocean crusts (Hein et al., 2000), is found in 35% CCM crusts and is not associated with phosphatization. It is thought that seawater around CCM seamounts did not become suboxic enough to encourage phosphatization in the crusts. Birnessite is a common accessory mineral and occurs in 5% of CCM Fe-Mn crusts; in contrast to open-ocean hydrogenetic crusts where it has not been detected.

Growth rates calculated by Co chronometer show increasing growth rates with increasing water depth both for the study area as a whole and to a greater extent for individual seamounts. This increase in growth rate with water depth is due to the increased supply of deeply sourced remobilized Fe and to a lesser extent Mn from continental shelf and slope sediments. This is the first study to document this water depth-growth rate relationship.

Elements of economic interest in Fe-Mn crusts are generally not as enriched in CCM samples as those from the PCZ crusts. Environmental concerns associated with extraction of crusts in a highly dynamic and productive environment need to be evaluated using best practices and the precautionary approach, as is true for all areas of the deep-ocean being considered for extraction of mineral resources.

Supplementary data to this article can be found online at http://dx.doi.org/10.1016/j.oregeorev.2016.09.010.

Acknowledgements

We would like to thank the Monterey Bay Aquarium Research Institute (MBARI) for providing samples and the opportunity to participate on research cruises to the study area. We thank the crew of the R.V. *Western Flyer* and the operators of the ROV *Doc Ricketts*. We would also like to thank Jenny Paduan, for help in sampling and data retrieval. We are also grateful to UCSC student Kristina Tu for her assistance with Arc GIS and sample preparation and UCSC student Natalie Zimdahl for her assistance with sample preparation. We would also like to thank Dr. Xiangwen, Dr. Katz Suzuki, and Mariah Mikesell for their thoughtful reviews.

References

Atwater, T., Severinghaus, J., 1989. Tectonic maps of the northeast Pacific, in the eastern Pacific Ocean and Hawaii. In: Winterer, E.L., Hussong, D.M., Decker, R.W. (Eds.), The Geology of North America — An Overview. Geological Society of America, Boulder, Colorado, pp. 265–297.

Banakar, V.K., Hein, J.R., Rajani, R.P., Chodankar, A.R., 2007. Platinum group elements and gold in ferromanganese crusts from Afanasiy-Nikitin seamount, equatorial Indian Ocean: sources and fractionation.

Bau, M., 1996. Controls on the fractionation of isovalent trace elements in magmatic and aqueous systems: evidence from Y/Ho, Zr/Hf, and lanthanide tetrad effect. Contrib. Mineral. Petrol. 123, 323–333. http://dx.doi.org/10.1007/s004100050159.

Bau, M., Schmidt, K., Koschinsky, A., Hein, J., Kuhn, T., Usui, A., 2014. Discriminating between different genetic types of marine ferro-manganese crusts and nodules based on rare earth elements and yttrium. Chem. Geol. 381, 1–9. http://dx.doi.org/10.1016/j.chemgeo.2014.05.004.

Berndmeyer, C., Birgel, D., Brunner, B., Wehrmann, L.M., Jöns, N., Bach, W., Arning, E.T., Föllmi, K.B., Peckmann, J., 2012. The influence of bacterial activity on phosphorite formation in the Miocene Monterey Formation. California. Palaeogeogr. Palaeoclimatol. Palaeoecol. 317–318, 171–181. http://dx.doi.org/10.1016/j.palaeo.2012.01.004.

Biller, D.V., Bruland, K.W., 2013. Sources and distributions of Mn, Fe, Co, Ni, Cu, Zn, and Cd relative to macronutrients along the central California coast during the spring and summer upwelling season. Mar. Chem. 155, 50–70. http://dx.doi.org/10.1016/j.marchem.2013.06.003.

Biller, D.V., Coale, T.H., Till, R.C., Smith, G.J., Bruland, K.W., 2013. Coastal iron and nitrate distributions during the spring and summer upwelling season in the central California Current upwelling regime. Cont. Shelf Res. 66, 58–72. http://dx.doi.org/10.1016/j.csr.2013.07.003.

Bonatti, E., Kraemer, T., Abdulla, H.A.N., 1972. Classification and genesis of submarine iron-manganese deposits. In: Horn, D.R. (Ed.), Ferromanganese Deposits on the Ocean Floor. National Science Foundation, Washington, D.C. USA, pp. 149–166.

Boyd, P.W., Ellwood, M.J., 2010. The biogeochemical cycle of iron in the ocean. Nat. Geosci. 3, 675–682. http://dx.doi.org/10.1038/ngeo964.

Broecker, W.S., Peng, T., Lamont-Doherty Geological Observatory, 1982. Tracers in the Sea. Eldigio Press, Palisades, N.Y.

Bruland, K.W., Lohan, M.C., 2003. Controls of trace metals in seawater. Treatise on Geochemistry. Elsevier, pp. 23–47.

Cande, S.C., Kent, D.V., 1995. Revised calibration of the geomagnetic polarity timescale for the Late Cretaceous and Cenozoic. J. Geophys. Res Solid Earth 100, 6093–6095. http://dx.doi.org/10.1029/94JB03098.

Carr, M.-E., 2001. Estimation of potential productivity in Eastern Boundary Currents using remote sensing. Deep Sea Res. Part II Top. Stud. Oceanogr. 49, 59–80. http://dx.doi.org/10.1016/S0967-0645(01)00094-7.

Chan, L.H., Edmond, J.M., Stallard, R.F., Broecker, W.S., Chung, Y.C., Weiss, R.F., Ku, T.L., 1976. Radium and barium at GEOSECS stations in the Atlantic and Pacific. Earth Planet. Sci. Lett. 32, 258–267. http://dx.doi.org/10.1016/0012-821X(76)90066-2.

Checkley, D.M., Barth, J.A., 2009. Patterns and processes in the California Current System. Prog. Oceanogr. 83, 49–64. http://dx.doi.org/10.1016/j.pocean.2009.07.028.

Chen, J.H., Lawrence Edwards, R., Wasserburg, G.J., 1986. ^{238}U, ^{234}U and ^{232}Th in seawater. Earth Planet. Sci. Lett. 80, 241–251. http://dx.doi.org/10.1016/0012-821X(86)90108-1.

Clague, D.A., Reynolds, J.R., Davis, A.S., 2000. Near-ridge seamount chains in the northeastern Pacific Ocean. J. Geophys. Res. Solid Earth 105, 16541–16561.

Clague, D.A., Paduan, J.B., Duncan, R.A., Huard, J.J., Davis, A.S., Castillo, P.R., Lonsdale, P., DeVogelaere, A., 2009. Five million years of compositionally diverse, episodic volcanism: construction of Davidson Seamount atop an abandoned spreading center: Davidson Seamount ages and glass chemistry. Geochem. Geophys. Geosyst. 10. http://dx.doi.org/10.1029/2009GC002665 n/a-n/a.

Coale, K.H., Bruland, K.W., 1987. Oceanic stratified euphotic zone as elucidated by ^{234}Th:^{238}U disequilibria. Limnol. Oceanogr. 32, 189–200. http://dx.doi.org/10.4319/lo.1987.32.1.0189.

Conway, T.M., John, S.G., 2015. The cycling of iron, zinc and cadmium in the North East Pacific Ocean — insights from stable isotopes. Geochim. Cosmochim. Acta 164, 262–283. http://dx.doi.org/10.1016/j.gca.2015.05.023.

Coumans, J.P., Stix, J., Clague, D.A., Minarik, W.G., 2015. The magmatic architecture of Taney Seamount-A, NE Pacific Ocean. J. Petrol. 56, 1037–1067. http://dx.doi.org/10.1093/petrology/egv027.

Davis, A.S., Gray, L.B., Clague, D.A., Hein, J.R., 2002. The Line Islands revisited: new $^{40}Ar/^{39}Ar$ geochronologic evidence for episodes of volcanism due to lithospheric extension: Line Islands revisited. Geochem. Geophys. Geosystems 3, 1–28. http://dx.doi.org/10.1029/2001GC000190.

Davis, A.S., Clague, D.A., Paduan, J.B., Cousens, B.L., Huard, J., 2010. Origin of volcanic seamounts at the continental margin of California related to changes in plate margins: origin of seamounts offshore California. Geochem. Geophys. Geosyst. 11. http://dx.doi.org/10.1029/2010GC003064 n/a-n/a.

Dickens, G.R., Owen, R.M., 1994. Late Miocene-Early Pliocene manganese redirection in the central Indian Ocean: Expansion of the Intermediate Water oxygen minimum zone. Paleoceanography 9, 169–181. http://dx.doi.org/10.1029/93PA02699.

ESRI, 2011. ArcGIS Desktop: Release 10. Environmental Systems Research Institute, Redlands, CA.

Filippelli, G.M., Delaney, M.L., Garrison, R.E., Omarzai, S.K., Behl, R.J., 1994. Phosphorus accumulation rates in a Miocene low oxygen basin: the Monterey Formation (Pismo Basin), California. Mar. Geol. 116, 419–430. http://dx.doi.org/10.1016/0025-3227(94)90055-8.

GEBCO, 2014. The GEBCO 2014 Grid, version 20150318. www.gebco.net.

Gibbs, A.E., Hein, J.R., Lewis, S.D., McCulloch, D.S., 1993. Hydrothermal palygorskite and ferromanganese mineralization at a central California margin fracture zone. Mar. Geol. 115, 19.

Halbach, P., Puteanus, D., 1984. The influence of the carbonate dissolution rate on the growth and composition of Co-rich ferromanganese crusts from Central Pacific seamount areas. Earth Planet. Sci. Lett. 68, 73–87. http://dx.doi.org/10.1016/0012-821X(84)90141-9.

Halbach, P., Segl, M., Puteanus, D., Mangini, A., 1983. Co-fluxes and growth rates in ferromanganese deposits from central Pacific seamount areas. Nature 304, 716–719. http://dx.doi.org/10.1038/304716a0.

Halbach, P.E., Sattler, C.-D., Teichmann, F., Wahsner, M., 1989. Cobalt rich and platinum bearing manganese crust deposits on seamounts: Nature, formation metal potential. Mar. Miner. 8, 23–39.

Hein, J.R., Koschinsky, A., 2014. Deep-ocean ferromanganese crusts and nodules. Treatise on Geochemistry. Elsevier, pp. 273–291.

Hein, J.R., Yeh, H.-W., Gunn, S.H., Sliter, W.V., Benninger, L.M., Wang, C.-H., 1993. Two major Cenozoic episodes of phosphogenesis recorded in equatorial Pacific seamount deposits. Paleoceanography 8, 293–311. http://dx.doi.org/10.1029/93PA00320.

Hein, J.R., Koschinsky, A., Bau, M., Manheim, F.T., Kang, J.-K., Roberts, L., 2000. Cobalt-rich ferromanganese crusts in the Pacific: chapter 9. Handbook of Marine Mineral Deposits. CRC Press, Boca Raton, Florida, pp. 239–279.

Hein, J.R., Koschinsky, A., McIntyre, B.R., 2005. Mercury- and silver-rich ferromanganese oxides, Southern California Borderland: deposit model and environmental implications. Econ. Geol. 100, 1151–1168. http://dx.doi.org/10.2113/gsecongeo.100.6.1151.

Hein, J.R., Zierenberg, R.A., Maynard, J.B., Hannington, M.D., 2007. Barite-forming environments along a rifted continental margin, Southern California Boderland. Deep Sea Res. Part II Top. Stud. Oceanogr. 54, 1327–1349. http://dx.doi.org/10.1016/j.dsr2.2007.04.011.

Hein, J.R., Conrad, T.A., Dunham, R.E., 2009. Seamount characteristics and mine-site model applied to exploration- and mining-lease-block selection for cobalt-rich ferromanganese crusts. Mar. Georesour. Geotechnol. 27, 160–176. http://dx.doi.org/10.1080/10641190902852485.

Hein, J.R., Conrad, T., Staudigel, H., 2010a. Seamount mineral deposits: a source of rare metals for high-technology industries. Oceanography 23, 184–189. http://dx.doi.org/10.5670/oceanog.2010.70.

Hein, J.R., Reid, J.A., Conrad, T.A., Dunham, R.E., Clague, D.A., Schulz, M.S., Davis, A.S., 2010b. Seamounts and ferromanganese crusts within and near the U.S. EEZ off California — data for RV Farnella cruise F7-87-SC (No. 2010-1069). U.S. Geological Survey.

Hein, J.R., Conrad, T.A., Frank, M., Christl, M., Sager, W.W., 2012. Copper-nickel-rich, amalgamated ferromanganese crust-nodule deposits from Shatsky Rise, NW Pacific: Shatsky Rise Cu-rich Fe-Mn crusts. Geochem. Geophys. Geosyst. 13. http://dx.doi.org/10.1029/2012GC004286 n/a-n/a.

Hein, J.R., Mizell, K., Koschinsky, A., Conrad, T.A., 2013. Deep-ocean mineral deposits as a source of critical metals for high- and green-technology applications: comparison with land-based resources. Ore Geol. Rev. 51, 1–14. http://dx.doi.org/10.1016/j.oregeorev.2012.12.001.

Hein, J.R., Conrad, T., Mizell, K., Banakar, V.K., Frey, F.A., Sager, W.W., 2016. Controls on ferromanganese crust composition and reconnaissance resource potential, Ninetyeast Ridge, Indian Ocean. Deep Sea Res. Part Oceanogr. Res. Pap. 110, 1–19. http://dx.doi.org/10.1016/j.dsr.2015.11.006.

Holt, J.W., Holt, E.W., Stock, J.M., 2000. An age constraint on Gulf of California rifting from the Santa Rosalia basin, Baja California Sur, Mexico. Geol. Soc. Am. Bull. 112, 540–549. http://dx.doi.org/10.1130/0016-7606(2000)112<540:AACOGO>2.0.CO;2.

Horner, T.J., Williams, H.M., Hein, J.R., Saito, M.A., Burton, K.W., Halliday, A.N., Nielsen, S.G., 2015. Persistence of deeply sourced iron in the Pacific Ocean. Proc. Natl. Acad. Sci. 112, 1292–1297. http://dx.doi.org/10.1073/pnas.1420188112.

Hsieh, Y.-T., Henderson, G.M., Thomas, A.L., 2011. Combining seawater ^{232}Th and ^{230}Th concentrations to determine dust fluxes to the surface ocean. Earth Planet. Sci. Lett. 312, 280–290. http://dx.doi.org/10.1016/j.epsl.2011.10.022.

Humayun, M., 2004. Geochemical evidence for excess iron in the mantle beneath Hawaii. Science 306, 91–94. http://dx.doi.org/10.1126/science.1101050.

Hyeong, K., Kim, J., Yoo, C.M., Moon, J.-W., Seo, I., 2013. Cenozoic history of phosphogenesis recorded in the ferromanganese crusts of central and western Pacific seamounts: Implications for deepwater circulation and phosphorus budgets. Palaeogeogr. Palaeoclimatol. Palaeoecol. 392, 293–301. http://dx.doi.org/10.1016/j.palaeo.2013.09.012.

Johnson, K.S., Coale, K.H., Berelson, W.M., Gordon, R.M., 1996. On the formation of the manganese maximum in the oxygen minimum. Geochim. Cosmochim. Acta 60, 1291–1299. http://dx.doi.org/10.1016/0016-7037(96)00005-1.

Johnson, K.S., Gordon, R.M., Coale, K.H., 1997. What controls dissolved iron concentrations in the world ocean? Mar. Chem. 57, 137–161. http://dx.doi.org/10.1016/S0304-4203(97)00043-1.

Johnson, H.P., Hautala, S.L., Bjorklund, T.A., Zarnetske, M.R., 2006. Quantifying the North Pacific silica plume: North Pacific silica plume. Geochem. Geophys. Geosyst. 7. http://dx.doi.org/10.1029/2005GC001065 n/a-n/a.

Klemm, V., Levasseur, S., Frank, M., Hein, J., Halliday, A., 2005. Osmium isotope stratigraphy of a marine ferromanganese crust. Earth Planet. Sci. Lett. 238, 42–48. http://dx.doi.org/10.1016/j.epsl.2005.07.016.

Klovan, J.E., Imbrie, J., 1971. An algorithm and FORTRAN-IV program for large-scale Q-mode factor analysis and calculation of factor scores. J. Int. Assoc. Math. Geol. 3, 61–77. http://dx.doi.org/10.1007/BF02047433.

Koschinsky, A., Halbach, P., 1995. Sequential leaching of marine ferromanganese precipitates: genetic implications. Geochim. Cosmochim. Acta 59, 5113–5132. http://dx.doi.org/10.1016/0016-7037(95)00358-4.

Koschinsky, A., Hein, J.R., 2003. Uptake of elements from seawater by ferromanganese crusts: solid-phase associations and seawater speciation. Mar. Geol. 198, 331–351. http://dx.doi.org/10.1016/S0025-3227(03)00122-1.

Koschinsky, A., Stascheit, A., Bau, M., Halbach, P., 1997. Effects of phosphatization on the geochemical and mineralogical composition of marine ferromanganese crusts. Geochim. Cosmochim. Acta 61, 4079–4094. http://dx.doi.org/10.1016/S0016-7037(97)00231-7.

Laurent, D., de Kaenel, E., Spangenberg, J.E., Föllmi, K.B., 2015. A sedimentological model of organic-matter preservation and phosphogenesis in the Miocene Monterey Formation at Haskells Beach, Goleta (central California). Sediment. Geol. 326, 16–32. http://dx.doi.org/10.1016/j.sedgeo.2015.06.008.

Lundsten, L., McClain, C., Barry, J., Cailliet, G., Clague, D., DeVogelaere, A., 2009. Ichthyofauna on three seamounts off southern and central California, USA. Mar. Ecol. Prog. Ser. 389, 223–232. http://dx.doi.org/10.3354/meps08181.

Mackey, D.J., O'Sullivan, J.E., Watson, R.J., Dal Pont, G., 2002. Trace metals in the Western Pacific: temporal and spatial variability in the concentrations of Cd, Cu, Mn and Ni. Deep Sea Res. Part Oceanogr. Res. Pap. 49, 2241–2259. http://dx.doi.org/10.1016/S0967-0637(02)00124-3.

Mangini, A., Key, R., 1983. A ^{230}Th profile in the Atlantic Ocean. Earth Planet. Sci. Lett. 62, 377–384. http://dx.doi.org/10.1016/0012-821X(83)90008-0.

Manheim, F.T., Lane-Bostwick, C.M., 1988. Cobalt in ferromanganese crusts as a monitor of hydrothermal discharge on the Pacific sea floor. Nature 335, 59–62. http://dx.doi.org/10.1038/335059a0.

Marsaglia, K.M., Davis, A.S., Rimkus, K., Clague, D.A., 2006. Evidence for interaction of a spreading ridge with the outer California borderland. Mar. Geol. 229, 259–272. http://dx.doi.org/10.1016/j.margeo.2006.02.006.

McLennan, S.M., 1989. Rare earth elements in sedimentary rocks; influence of provenance and sedimentary processes. In: Lipin, B.R., McKay, G.A. (Eds.), Geochemistry and Mineralogy of Rare Earth ElementsRev. in Mineralogy. Mineralogical Society of America, Washington, D.C., USA, pp. 169–200.

McManus, J., Berelson, W.M., Severmann, S., Johnson, K.S., Hammond, D.E., Roy, M., Coale, K.H., 2012. Benthic manganese fluxes along the Oregon–California continental shelf and slope. Cont. Shelf Res. 43, 71–85. http://dx.doi.org/10.1016/j.csr.2012.04.016.

Morel, F.M.M., Milligan, A.J., Saito, M.A., 2014. Marine bioinorganic chemistry: the role of trace metals in the oceanic cycles of major nutrients. Treatise on Geochemistry. Elsevier, pp. 123–150.

Muiños, S.B., Hein, J.R., Frank, M., Monteiro, J.H., Gaspar, L., Conrad, T., Pereira, H.G., Abrantes, F., 2013. Deep-sea Fe-Mn crusts from the northeast Atlantic Ocean: composition and resource considerations. Mar. Georesources Geotechnol. 31, 40–70. http://dx.doi.org/10.1080/1064119X.2012.661215.

Nozaki, Y., Yang, H.-S., Yamada, M., 1987. Scavenging of thorium in the ocean. J. Geophys. Res. 92, 772. http://dx.doi.org/10.1029/JC092iC01p00772.

Oskin, M., Stock, J., 2003. Pacific–North America plate motion and opening of the Upper Delfín basin, northern Gulf of California. Mexico. Geol. Soc. Am. Bull. 115, 1173. http://dx.doi.org/10.1130/B25154.1.

Paduan, J.B., Clague, D.A., Davis, A.S., 2009. Evidence that three seamounts off southern California were ancient islands. Mar. Geol. 265, 146–156. http://dx.doi.org/10.1016/j.margeo.2009.07.003.

Paytan, A., Griffith, E.M., 2007. Marine barite: recorder of variations in ocean export productivity. Deep Sea Res. Part II Top. Stud. Oceanogr. 54, 687–705. http://dx.doi.org/10.1016/j.dsr2.2007.01.007.

Paytan, A., Mearon, S., Cobb, K., Kastner, M., 2002. Origin of marine barite deposits: Sr and S isotope characterization. Geology 30, 747. http://dx.doi.org/10.1130/0091-7613(2002)030<0747:OOMBDS>2.0.CO;2.

Pisias, N.G., Murray, R.W., Scudder, R.P., 2013. Multivariate statistical analysis and partitioning of sedimentary geochemical data sets: general principles and specific MATLAB scripts: technical brief. Geochem. Geophys. Geosystems 14, 4015–4020. http://dx.doi.org/10.1002/ggge.20247.

Powell, R.E., Weldon, R.J., 1992. Evolution of the San Andreas Fault. Annu. Rev. Earth Planet. Sci. 20, 431–468. http://dx.doi.org/10.1146/annurev.ea.20.050192.002243.

Puteanus, D., Halbach, P., 1988. Correlation of Co concentration and growth rate — a method for age determination of ferromanganese crusts. Chem. Geol. 69, 73–85. http://dx.doi.org/10.1016/0009-2541(88)90159-3.

Qin, L., Humayun, M., 2008. The Fe/Mn ratio in MORB and OIB determined by ICP-MS. Geochim. Cosmochim. Acta 72, 1660–1677. http://dx.doi.org/10.1016/j.gca.2008.01.012.

Rajani, R.P., Banakar, V.K., Parthiban, G., Mudholkar, A.V., Chodankar, A.R., 2005. Compositional variation and genesis of ferromanganese crusts of the Afanasiy–Nikitin Seamount, Equatorial Indian Ocean. J. Earth Syst. Sci. 114, 51–61. http://dx.doi.org/10.1007/BF02702008.

Rowden, A.A., Dower, J.F., Schlacher, T.A., Consalvey, M., Clark, M.R., 2010. Paradigms in seamount ecology: fact, fiction and future: paradigms in seamount ecology. Mar. Ecol. 31, 226–241. http://dx.doi.org/10.1111/j.1439-0485.2010.00400.x.

Roy-Barman, M., Chen, J.H., Wasserburg, G.J., 1996. ^{230}Th—^{232}Th systematics in the central Pacific Ocean: the sources and the fates of thorium. Earth Planet. Sci. Lett. 139, 351–363. http://dx.doi.org/10.1016/0012-821X(96)00017-9.

Rudnick, R.L., Gao, S., 2014. Composition of the continental crust. Treatise on Geochemistry. Elsevier, pp. 1–51.

Ryan, W.B.F., Carbotte, S.M., Coplan, J.O., O'Hara, S., Melkonian, A., Arko, R., Weissel, R.A., Ferrini, V., Goodwillie, A., Nitsche, F., Bonczkowski, J., Zemsky, R., 2009. Global Multi-Resolution Topography synthesis. Geochem. Geophys. Geosyst. 10, Q03014. http://dx.doi.org/10.1029/2008GC002332.

Talley, L.D., 2008. Freshwater transport estimates and the global overturning circulation: shallow, deep and throughflow components. Prog. Oceanogr. 78, 257–303. http://dx.doi.org/10.1016/j.pocean.2008.05.001.

Talley, L.D., Joyce, T.M., 1992. The double silica maximum in the North Pacific. J. Geophys. Res. 97, 5465. http://dx.doi.org/10.1029/92JC00037.

Taylor, S.R., McLennan, S.M., 1985. The continental crust: its composition and evolution. Geol. Mag. 122, 673. http://dx.doi.org/10.1017/S0016756800032167.

White, W.M., Klein, E.M., 2014. Composition of the oceanic crust. Treatise on Geochemistry. Elsevier, pp. 457–496.